AD-A073 457 NAVAL POSTGRADUATE SCHOOL MONTEREY CA F/G 20/11
VIBRATION ANALYSIS AND NONDESTRUCTIVE TESTING USING DOUBLE-EXPO--ETC(U)
JUN 79 J M FAHEY

UNCLASSIFIED NL

1 OF 2
AD A073457

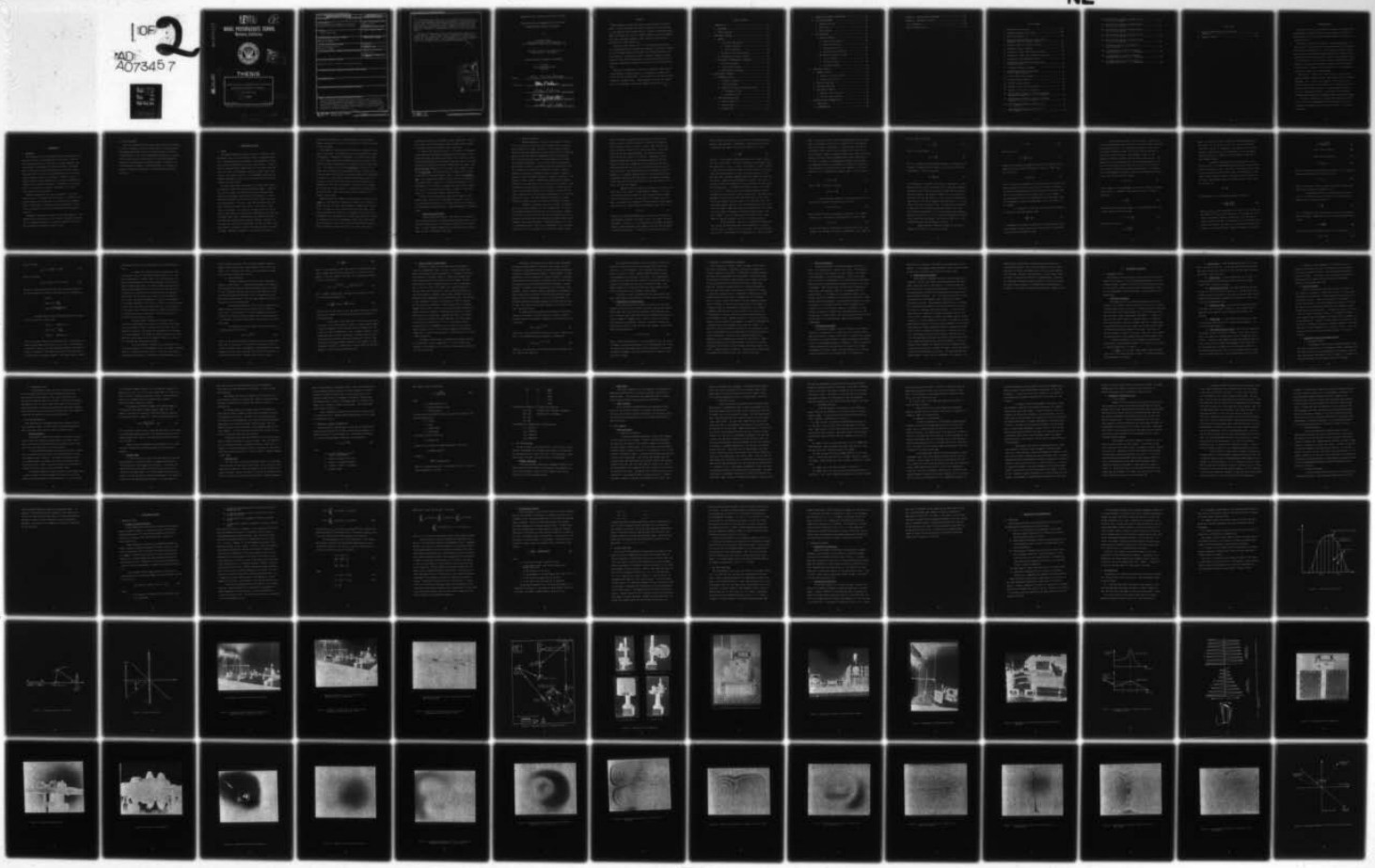

LEVEL II

AD A073457

NAVAL POSTGRADUATE SCHOOL

Monterey, California

DDC FILE COPY

DDC RECEIVED AUG 31 1979 C

(9) Master's THESIS,

(6) VIBRATION ANALYSIS AND NONDESTRUCTIVE TESTING USING DOUBLE-EXPOSURE HOLOGRAPHIC TECHNIQUES.

(10) John Michael Fahey

(11) June 1979

(12) 112 p.

Thesis Advisor: A. E. Fuhs

Approved for public release; distribution unlimited.

79 08 31 025

251 450 bpg

SECURITY CLASSIFICATION OF THIS PAGE (When Data Entered)

REPORT DOCUMENTATION PAGE		READ INSTRUCTIONS BEFORE COMPLETING FORM
1. REPORT NUMBER	2. GOVT ACCESSION NO.	3. RECIPIENT'S CATALOG NUMBER
4. TITLE (and Subtitle) Vibration Analysis and Nondestructive Testing Using Double-Exposure Holographic Techniques		5. TYPE OF REPORT & PERIOD COVERED Master's Thesis; June 1979
		6. PERFORMING ORG. REPORT NUMBER
7. AUTHOR(s) John Michael Fahey		8. CONTRACT OR GRANT NUMBER(s)
9. PERFORMING ORGANIZATION NAME AND ADDRESS Naval Postgraduate School Monterey, CA 93940		10. PROGRAM ELEMENT, PROJECT, TASK AREA & WORK UNIT NUMBERS
11. CONTROLLING OFFICE NAME AND ADDRESS Naval Postgraduate School Monterey, CA 93940		12. REPORT DATE June 1979
		13. NUMBER OF PAGES 111
14. MONITORING AGENCY NAME & ADDRESS(if different from Controlling Office)		15. SECURITY CLASS. (of this report) Unclassified
		15a. DECLASSIFICATION/DOWNGRADING SCHEDULE

16. DISTRIBUTION STATEMENT (of this Report)

Approved for public release; distribution unlimited.

17. DISTRIBUTION STATEMENT (of the abstract entered in Block 20, if different from Report)

18. SUPPLEMENTARY NOTES

19. KEY WORDS (Continue on reverse side if necessary and identify by block number)

20. ABSTRACT (Continue on reverse side if necessary and identify by block number)

Double-exposure holograms were made of aluminum 2024-T4 rectangular plates. The double-exposure technique was applied to an aluminum plate in a nonflawed and then a flawed condition. Results of these experiments, comparing the effects at various resonant frequencies, were then compared with results previously obtained in other studies to ascertain their applicability to Naval Engineering.

DD FORM 1 JAN 73 1473 EDITION OF 1 NOV 65 IS OBSOLETE
S/N 0102-014-6601 |
(Page 1)

SECURITY CLASSIFICATION OF THIS PAGE (When Data Entered)

The plate was then flawed with a 1 inch through-thickness vertical slit, and double-exposure holograms were generated. The resonant frequencies of the flawed plates were recorded, and the mode shape deviations were analyzed. A comparison was made of resonant frequencies and mode shapes of flawed and nonflawed plates to determine the applicability of holographic procedures to nondestructive testing of vibrating mechanical parts.

Results of the experiments indicate that holographic nondestructive testing (HNDT) of vibrating objects in a shipboard environment holds promise for future applications. Further research is required to develop systems for use aboard ships. These procedures are being used successfully in the aerospace industry and automobile manufacturing.

Accession For
NTIS GRA&I
DDC TAB
Unannounced
Justification
By
Distribution/
Availability Codes
Dist | Avail and/or special
A

79 08 31 025

Approved for public release; distribution unlimited.

VIBRATION ANALYSIS AND NONDESTRUCTIVE TESTING USING DOUBLE-EXPOSURE HOLOGRAPHIC TECHNIQUES

by

John Michael Fahey
Lieutenant Commander, United States Navy
B.A., University of Tennessee at Chattanooga, 1966

Submitted in partial fulfillment of the
requirements for the degree of

MASTER OF SCIENCE IN MECHANICAL ENGINEERING

from the

NAVAL POSTGRADUATE SCHOOL
June 1979

Author John Michael Fahey

Approved by: Allen E Fuhs
Thesis Advisor

Arthur P. Boresi
Second Reader

R. J. Martin
Chairman, Department of Mechanical Engineering

William M. Tolles
Dean of Science and Engineering

ABSTRACT

Double-exposure holograms were made of aluminum 2024-T4 rectangular plates. The double-exposure technique was applied to an aluminum plate in a nonflawed and then a flawed condition. Results of these experiments, comparing the effects at various resonant frequencies, were then compared with results previously obtained in other studies to ascertain their applicability to Naval Engineering.

The plate was then flawed with a 1 inch through-thickness vertical slit, and double-exposure holograms were generated. The resonant frequencies of the flawed plates were recorded, and the mode shape deviations were analyzed. A comparison was made of resonant frequencies and mode shapes of flawed and nonflawed plates to determine the applicability of holographic procedures to nondestructive testing of vibrating mechanical parts.

Results of the experiments indicate that holographic nondestructive testing (HNDT) of vibrating objects in a shipboard environment holds promise for future applications. Further research is required to develop systems for use aboard ships. These procedures are being used successfully in the aerospace industry and automobile manufacturing.

TABLE OF CONTENTS

LIST OF FIGURES

LIST OF TABLES

ACKNOWLEDGEMENTS

The author would like to acknowledge the support of the Naval Postgraduate School Foundation Research Program funded by the Office of Naval Research, for providing the equipment necessary to conduct this research project.

Most of all I would like to express my sincere appreciation to my thesis advisor, Dr. Allen E. Fuhs, Distinguished Professor of Mechanical and Aeronautical Engineering. Dr. Fuhs' technical guidance, unselfish devotion to duty, patience and unparalleled ability to make difficult concepts seem simple were the guiding factors to the successful completion of the project. Also I am very grateful to have had the distinct pleasure of having had the professional expertise of Distinguished Professor Arthur P. Boresi of the University of Illinois, NAVSEA Research Chair Professor, as a second reader.

Additionally, I would like to thank Mrs. Vicki Culley for her logistical support without which the investigation would not have been completed. Also, I would like to thank Mr. Tom Christian for his technical support and Mr. Ken Mothersell for his expeditious and professional machine shop assistance. The professional and unselfish aid of Mr. Howard Bensch and Mr. Arthur Murray of the Educational Media Department Photo Lab was commendable and sincerely appreciated.

This thesis is dedicated to the unparalleled educational ability of Dr. Fuhs and the indefatigable devotion and support of my wife throughout my graduate studies and my entire career in the United States Navy.

I. INTRODUCTION

A. BACKGROUND

With the advent of the Helium-Neon gas laser and holographic procedures, the field of vibrational analysis was altered in 1964 [1]. This marked the beginning of man's ability to see, photograph, and analyze exactly the contours of vibration amplitudes. Holography permits measurement of surface displacements at two length scales. One length scale is in units of the wavelength of light. The other ranges from tens of microns to millimeters. Defects or flaws in material objects suitably loaded usually will manifest themselves as abnormalities in surface displacement. For example, a small crack, which is a discontinuity in material properties, will alter the strain pattern of the test object.

Numerous advantages for the use of holography in vibrational analysis exist in our complex technical society. By vibrating an object and generating its hologram, one is provided with a permanent record of that object's vibration contours and amplitude. The use for this technique in aircraft and ship machinery has considerable potential.

Holographic techniques also appear to have great potential in the nondestructive testing industry. By vibrating a specimen and analyzing its subsequent hologram at its resonant frequencies, one may be able to determine the nature of material flaws.

B. THESIS OBJECTIVE

The primary objectives of this thesis were to apply the techniques of optical holography to the vibrational analysis of aluminum plates and compare experimental results with those theoretical results obtained by others in the fields of holography and vibrations. Coupled with vibrational analysis, the feasibility of applying holographic techniques to nondestructive testing was studied. The objective for using holographic procedures in Naval Engineering is to improve the accuracy of measuring deficiencies in shipboard machinery and hull structures.

II. EXPERIMENTAL METHODS

A. GENERAL

The standard photographic process records in illuminated three-dimensional scene as a two-dimensional image on a photographic emulsion. The hologram which can reproduce a three-dimensional picture can be called a photograph by wave front reconstruction. It does not record an image but rather records reflected light waves from an object. The result is a photographic record that looks like an array of fuzzy lines, blobs, and swirls. This hodgepodge record does not resemble the image but rather is an optical code which cannot be recorded by any other process.

The idea of holography was discovered by Professor Denis Gabor of the Imperial College of Science and Technology, London, in 1948 [1]. At the time Dr. Gabor was investigating ways to reduce spherical aberration in high-magnification electron microscopes [2]. He conducted his experiments with light from a mercury vapor lamp using a very small aperture. The mercury vapor lamp was coherent but very weak. After the invention of the laser, it was used as a light source in holography. Utilization of the laser at the light source gives a more intense and a more coherent monochromatic light than does the mercury vapor lamp. Professor Gabor gave the name "hologram" to the picture he obtained, and the name has remained. Stemming from the Greek root "holos", which means whole, and the word "gram", which means measure, a hologram is essentially a complete record of a scene or object. Therefore, holography is the science of recording an

entire optical wavefront on a suitable material, usually a photographic plate, and of utilizing the information so recorded to analyze physical phenomena.

The concepts of refraction and diffraction are of paramount importance in holography. To understand this, one must consider the nature of holography. Fundamental in holography is a suitable light source. As is well known, light from a distant source such as the sun can be brought into focus by concentrating it through a lens to a small focal spot. This process which is called refraction is the basis of all common imaging systems such as eyeglasses, cameras, binoculars, etc. Light rays actually are bent by a transparent object during the process of refraction. A part of the illuminating laser beam is bent or deflected to a bright focal point, just as with the refracting lens. Another part of the light is deflected in such a way that is spreads out from the rear of the plate as if it had come from a focal spot in front of the plate. Some of the original beam just passes on as if through a glass window.

Another type of lens depends on diffraction only. Recall the star (smear) of light observed by looking at a distant light through a pin hole or narrow slit. While the diffraction of common white light will result in a smear of light, the diffraction of a laser beam is precisely predictable and controlled. For example, one may have used a photographic plate and exposed it to a laser beam, having first placed in the beam and in front of photographic plate a small round object such as the head of a pin. Laser light striking the head of the pinhead is scattered to the plate; but as it arrives on the plate, it

interferes with that part of the beam which was undeflected by the pinhead. Just as with interferometry, these two beams create a pattern of alternate bright and dark bands fixed on the plate.

As simple as this process may seem, it is the basis of holography. Unlike conventional photography, holography does not require a lens. Instead both phase and amplitude information are recorded as a result of the interference pattern formed when light waves are split and then rejoined after some portion has been reflected from the object. The part of the beam reflected off of the object onto the plate is known as the object beam. The remaining part of the beam, that is transmitted directly to the photographic plate, is called the reference beam. Once recorded, the hologram itself will bear no resemblance to the recorded object. However, by illuminating the hologram in the same manner as it was originally exposed, the object may be viewed as if it were in its original position and will retain its three dimensionality. This process is known as reconstruction.

In order to form high-contrast interference fringes on a holographic plate, three distinct requirements must be met. They are (1) Light Source Requirements, (2) Vibration Stability Requirements, (3) Photographic Plate Requirements. These requirements are discussed below.

1. Light Source Requirements

The most common and important light source for holography today is the gas laser [3]. The double-exposure holograms taken in this work were accomplished with a Helium-Neon laser with a 5 millimeter beam. The most important properties of the light source are the temporal and spatial coherence of the light.

a. Temporal Coherence

Temporal coherence is a measure of the degree of correlation of a wave at one time with a wave at another time. By taking a wave at some point in space, splitting in into two parts, delaying one portion and then recombining, the two portions form an interference pattern by which the temporal coherence of a wave can be measured. For this reason the pulse nature of the Helium-Neon laser is ideal for holographic techniques. The light source used for holographic applications must exhibit long temporal coherence characteristics and must, therefore, be essentially a monochromatic source. Temporal coherence, most commonly expressed in units of length, is actually a measure in time of the phase consistency of successive wavefronts. The temporal coherence length is determined by multiplying the temporal coherence time by the speed of light, thus the units of length. Since the temporal coherence length of a light source is inversely proportional to the frequency bandwidth of the source, it follows that the longest lengths possible are achieved by monochromatic or a single frequency light source. The laser, generally considered to be monochromatic, provides the best light source for holographic purposes.

Basically, a gas laser consists of an atomic or molecular gas at low pressure contained in a long discharge tube. The axis of the discharge tube defines the optical axis of the system. Centered on this axis, at each end of the tube, are high-reflectivity mirrors, aligned so that light traveling along the axis reflects back and forth numerous times through the medium. A small percentage of this light is transmitted by one or both mirrors on each pass. This transmission represents a loss to the system, so for relatively low-gain lasers,

such as the He-Ne, high quality, high-reflectivity mirrors are required. The gas is excited by means of an electrical discharge at radio frequencies, direct current, or pulsed. Under certain conditions a population inversion within the gas may exist. Under these conditions the gas discharge becomes a light amplifier for the transition for which there is an inversion. Spontaneous emission causes stimulated emission, and the process cascades as the light travels along the tube. Because of this inversion, amplification of spontaneous emission results as the light reflects back and forth between the mirrors. The random nature of the spontaneous emissions is swamped by the in-phase, coherent nature of the stimulated emissions. The temporal coherence of the light output is quite high; but because of the nature of the amplifying transition, most laser beams are not single, but multiple frequency.

Because of the low pressure of the gas in a gas laser, the transition line of interest is always Doppler broadened. This line, wich normally would be an absorption line, becomes the gain envelope when an inversion exists. Thus the laser is a resonant cavity with gain. The condition for resonance is that the round-trip path between the mirrors be an integral number of wavelengths, shown in eqn. (1):

$$2d = m\lambda \tag{1}$$

where d is the distance between the laser mirrors (cavity length), λ is the wavelength at Doppler line center, and m is an integer, the axial mode number. Since $d \gg \lambda$, it is possible that the separation between adjacent allowed resonances (axial modes) may be less than the Doppler linewidth (gain envelope). If the gain is sufficiently high, more

than one mode may oscillate at once, yielding a multifrequency output. The axial mode separation is determined by calculating the variation in wavelength that changes the axial mode number by unity. Thus

$$\Delta\lambda_c = \frac{\lambda^2}{2d} \tag{2}$$

where $\Delta\lambda_c$ is the wavelength separation between cavity modes. Hence if the laser is oscillating in a mode of wavelength λ, the adjacent allowable modes are at $\lambda \pm \Delta\lambda_c$. A typical laser spectrum is shown in Figure 1. Note that for the situation shown, only three modes will oscillate since the allowable modes at $\lambda \pm 2\Delta\lambda_c$ fall below threshold. If the gain were to be increased, subsequent additional modes would come into oscillation. Because of the mode separation relation, (Eqn. 2), it is possible to obtain single-mode operation by shortening the laser cavity. For the He-Ne laser, $\lambda = 0.6328$ and the Doppler width is of the order of 1.8×10^{-6} μ. Hence the axial mode wavelength separation equals the Doppler width for a cavity length of about 10 cm. The He-Ne system possesses sufficient gain so that single-mode lasers of this length can be made. However, the power output will be relatively small, and single-mode operation does not imply single-frequency operation, since the single mode may wander about under the gain envelope. This wandering may be caused, for example, by thermally induced changes in the cavity length. In order to obtain more useful power levels, longer lasers are generally employed, resulting in a multimode output.

Since holography is basically a two-beam interference problem, consider the simple experiment shown schematically in Figure 2. The laser cavity is formed by mirrors M_1 and M_2. The light transmitted by M_2 is split into two beams at the beamsplitter S. One of the beams,

beam 1, travels to the point P on the recording medium, and the other, beam 2, is reflected by the mirror R to the point P. The angle between the two beams is denoted by ϕ. These two beams interfere at the plate in the x-y plane, forming straight-line fringes lying in the x-direction. However, exposure of these fringes requires a finite exposure time and all optical components must remain steady during this time. In general, a time-dependent wavelength from the laser, a time-dependent optical path difference D = SRP-SP, or a stable but multimode laser will cause smearing of the fringes at P. For small angles, $\sin \phi = \phi$; therefore, the phase of beam 1 in the x direction is

$$\delta_1(x) = kx \frac{\phi}{2} \tag{3}$$

where $k = \frac{2\pi}{\lambda}$. Similarly, for beam 2

$$\delta_2(x) = -kx \frac{\phi}{2} \tag{4}$$

One of the waves (beams) will have traveled an extra distance D, and the phase difference along x will be

$$\delta(x) = k(D + x\phi) \tag{5}$$

Now a bright fringe will be produced at x when $\delta(x)$ is an integral multiple of 2π. This leads to the condition for a bright fringe

$$D + x\phi = m\lambda \tag{6}$$

Here m is the order of interference; its average value is D/λ. Now suppose a small change $\Delta\lambda$ is made in the wavelength. The fringes will

shift an amount Δx given by

$$\Delta x = m \frac{\Delta\lambda}{\phi} \tag{7}$$

with $m = D/\lambda$, eqn. becomes

$$\Delta x = \Delta\lambda \frac{D}{\lambda\phi} \tag{8}$$

But $\phi = \lambda\nu_f$ relates the angle between the beams, the wavelength, and the spatial frequency of the fringes, ν_f. Let $\Delta x_f = 1/\nu_f$ for the fringe spacing. Then eqn. (8) yields

$$\Delta x = \frac{\Delta\lambda}{\lambda^2} D\Delta x_f \tag{9}$$

as the distance a fringe moves for a change in wavelength $\Delta\lambda$. Most commercial lasers used for holography are not stabilized completely. Consequently, small thermal variations can cause important changes in the cavity length d. For example a change in d of $\lambda/2$ results in a wavelength shift for each mode of $\Delta\lambda = \Delta\lambda_c$. For a well-constructed laser thermal drifts are not expected to be such that $\lambda \rightarrow \lambda + \Delta\lambda_c$ for times of the order of seconds or less. In some lasers the situation is much worse, with the modes jumping about randomly and rapidly. For a change in wavelengths of $\Delta\lambda = \Delta\lambda_c$, the laser output spectrum is identical to that for $\Delta\lambda = 0$. As a result, wavelength shifts greater than $\Delta\lambda_c$ need not be considered. The effect of these shifts on the interference pattern can be analyzed as follows:

Suppose the path difference D between the two beams is expressed as a fraction of the cavity length d:

$$D = Kd \tag{10}$$

Then, by eqn. (9),

$$\Delta x = \frac{\Delta\lambda_c}{\lambda^2} Kd\ \Delta x_f \tag{11}$$

Equation (11) expresses the change in position of a fringe for a wavelength shift $\Delta\lambda_c$ and a path difference Kd. But $\Delta\lambda_c = \lambda^2/2d$. Hence eqn. (11) yields

$$\Delta x = \frac{1}{2} K\ \Delta x_f \tag{12}$$

Thus it is seen that an expansion of the laser cavity by $\lambda/2$ causes the output spectrum to shift by $\Delta\lambda_c$ resulting in a fringe displacement Δx. For a path difference between the two beams equal to the cavity length D(K = 1), the fringes shift by an amount $\Delta x_f/2$. If this happens during one exposure time, the fringe pattern on the photographic plate will be essentially completely demodulated, that is, no fringes will be recorded.

It is important to note that the fringe shift expressed as a fraction of the fringe spacing, namely

$$\frac{\Delta x}{\Delta x_f} = \frac{1}{2} K \tag{13}$$

is independent of the spatial frequency of the fringe pattern; hence high-frequency fringes (large ϕ) are no more sensitive to wavelength variation than low-frequency fringes.

Next, consider the case in which the laser is operating at a single wavelength that does not drift in time (single mode, stabilized), and examine the effect on the interference fringes of a time-varying optical path difference. Recall from Figure 2 that the two beams of light travel different paths to the photographic plate. A time-dependent difference in the paths that the beams travel may occur. For example, such a difference can result from unequal temperatures in the two arms which change in time from slight air drafts in the room, or from vibration of the mirror and beam splitter supports. The effects of this time-dependent difference in paths can be analyzed with the aid of eqn. (6). Thus for a bright fringe,

$$D + x\phi = m\lambda \tag{14}$$

A small change in the time-dependent optical path difference D, denoted by ΔD, results in a change in fringe position by eqn. (14) equal in magnitude to

$$\Delta x = \frac{\Delta D}{\phi} \tag{15}$$

where the minus sign has been dropped. It has been assumed that λ and m remain constant with the relations,

$$\phi = \lambda \nu_f = \frac{\lambda}{\Delta x_f} \tag{16}$$

and Δx may be written as

$$\Delta x = \frac{\Delta x_f \, \Delta D}{\lambda} \tag{17}$$

Hence, it is seen that there is essentially complete demodulation of the fringes (i.e. $\Delta x = \frac{1}{2} \Delta x_f$), for $\Delta D = \lambda/2$. Also the fractional fringe shift, $\Delta x/\Delta x_f$, is independent of the frequency of the fringes. Here again, the sensitivity of the modulation of the fringe system to path variations is no greater for high-frequency fringes than for low-frequency fringes.

To examine the modulation of the fringe pattern with a multimode laser, it is assumed that both mode position and path difference are stationary in time. A gas laser of sufficient gain oscillates in more than one longitudinal (axial) mode if the separation of these modes is smaller than the width of the atomic line of the transition involved. The wavelength separation of adjacent axial modes is given by; see eqn. (2),

$$\Delta\lambda_c = \frac{\lambda^2}{\Delta\lambda}$$

The modulation M of an interference pattern is defined as

$$M \equiv \frac{I_{max} - I_{min}}{I_{max} + I_{min}} \tag{18}$$

where I_{max} and I_{min} are, respectively, the values of the irradiance at the maxima and minima of the fringe pattern. This modulation is related to the spectral intensity distribution of the light source through a Fourier transform. A discussion of this relationship may be found in Born and Wolf [4], where it is shown that the modulation of fringes of two interfering beams of equal irradiance can be written:

$$M = \frac{(S^2 + C^2)^{1/2}}{P} \tag{19}$$

$$S(D) = 2\int j(x) \sin(xD)\, dx \tag{20}$$

$$C(D) \equiv 2\int j(x) \cos(xD)\, dx \tag{21}$$

$$P \equiv 2\int j(x)\, dx \tag{22}$$

Here D is the optical path difference as before, $j(x)$ is the spectral intensity distribution of the light source, and

$$x = k - k_o \tag{23}$$

where $k = 2\pi/\lambda$ and $k_o = 2\pi/\lambda_o$, λ_o being an arbitrarily chosen wavelength near the center of the Doppler line.

A good approximation to a multimode gas laser source is that $j(x)$ is a sum of Dirac delta functions $\delta(x)$, with each spike separated from its nearest neighbor by

$$\Delta k = \frac{2\pi}{2d} \tag{24}$$

If it is assumed also that the spectral distribution is symmetrical about line center. Hence, $S(D) = 0$ and the fringe modulation can be written

$$M = \frac{|C(D)|}{P} \tag{25}$$

For the delta-function spectrum, we have, for a single mode.

$$j_1(x) = \delta(x) \tag{26}$$

and for two modes

$$j_2(x) = \delta(x - \frac{\Delta k}{z}) + \delta(x + \frac{\Delta k}{z}) \tag{27}$$

and for three modes

$$j_3(x) = \delta(x-\Delta k) + \delta(x) + \delta(x+\Delta k) \tag{28}$$

and so on. With these expressions for $j_n(x)$, the fringe modulation M_n, where n denotes the number of modes oscillating, is expressed by,

$$M_1(D) = 1$$

$$M_2(D) = \left|\cos\ (\frac{\pi D}{2d})\right|$$

$$M_3(D) = \frac{|2\ \cos(\Delta k D) + 1|}{3}$$

Evaluating these for path differences equal to an integer multiple of the cavity length yields

$$M_n(o) = 1 \quad \text{regardless of n}$$

$$M_n(d) = \begin{cases} 1 & \text{n odd} \\ 0 & \text{n even} \end{cases}$$

$$M_n(2d) = 1 \quad \text{regardless of n}$$

Thus for zero path difference the fringe modulation is 100 percent no matter how many modes are oscillating. For a path difference equal to one cavity length d, the fringe modulation depends on the number of modes; for example, if three modes are oscillating, the modulation is 1/3, assuming all have equal strength. In any actual laser, of course,

the modes may not be of equal strength and must be weighed accordingly.

In summary, the problem of forming interference fringes with gas laser light for three cases has been examined: (1) a time-varying wavelength in the laser output, (2) a time-varying optical path difference between the two interfering beams, and (3) a multimode but stable laser output. All three of these perturbations can cause a serious demodulation of the fringes with a resultant loss in diffracted flux or possibly even a complete loss of the hologram. These effects can, of course, occur singly or in any combination. In all cases, the degree of demodulation is found to be independent of the spatial frequency of the fringes. Problem (1) can be eliminated by working near zero path difference; problem (2), by stabilization of the supports and by blocking possible air drafts; and problem (3), by working hear zero path difference or a path difference that is an even multiple of the cavity length.

A nonzero spectral bandwidth of the source used for illuminating the hologram mainly affects the resultant image resolution, as discussed previously. Because of this, the gas laser still represents the optimum illuminating source because of its high power in a narrow bandwidth. Even though the effective bandwidth of a multimode laser must be taken as the full Doppler width, this is usually still narrower than most spectral sources.

Since the hologram is formed by the interference of two light waves converging on the photographic plate, the temporal coherence length is an extremely important factor. For optimum high-contract holograms, the path lengths of the object and reference beams must be

as nearly equal as possible. With an extended temporal coherence length, such as with the laser, these paths may vary as much as two inches. With a standard light source, on the other hand, the beams would have to be matched within microns.

b. Spatial Coherence

The spatial coherence of the light used in holography is important in two respects. In recording the hologram, both reference and object beams must have well-defined wavefronts that are constant in time. The object wave may, of course, be highly complex in shape but should nevertheless be constant. Also, in reconstructing the object wave, the resolution in the final image depends on the size of the source of the illuminating wave.

The spatial coherence of a light field is a measure of the degree of phase correlation at two different points of space at a single time. This correlation is primarily dependent on the size of the source from which the light originated; to find phase correlation it is necessary to know the precise spatial distribution of flux from a gas laser.

The lowest-order (spatial) model from a gas laser has an irradiance variation of the form

$$I(\rho) \approx I_o e^{2\rho^2/w} \tag{29}$$

where ρ is the radial distance from the axis and w is called the spot size, that is, the value of ρ at which the irradiance has fallen to $1/e^2$ of its central value. The wavefront is either spherical or plane. Suppose one wishes to focus the laser light with this distribution to a small point with a lens. The spot size at focus is given by

$$w_o = \frac{\lambda}{\tau N.A.} \tag{30}$$

where λ is the wavelength of the light and N.A. is the numerical aperture of thelens used to focus the light, which in this case is w/f, where f is the focal length of the lens. The irradiance distribution at focus is thus given by

$$I(\rho) = I_o e^{-2\rho^2/w_o^2} = I_o e^{-2\pi^2\rho^2(N.A.)^2/\lambda^2} \tag{31}$$

For $\lambda = 0.6328\ \mu$ (He-Ne laser), the spot size as a function of the N.A. of the focusing objective is

$$w_o = \frac{0.2}{N.A.} \text{ microns} = \frac{0.2f}{w} \text{ microns} \tag{32}$$

assuming that the spot size w of the light entering the lens is smaller than the lens diameter. This spot size determines the resolution in the reconstruction.

For the case in which more than a single transverse mode is oscillating, the situation worsens. Not only is there a smaller degree of spatial coherence, but also the beam cannot be focused to as small a spot as in the single-mode case. Thus, in general, whenever a single, higher-order mode or several higher-order transverse modes are oscillating, both the diffraction efficiency (because of a smaller fringe contrast) of the hologram andthe resolution in the image will suffer. Fortunately virtually all commercially available lasers are designed to operate in a single low-order transverse mode.

2. Vibration Stability Requirements

Holography is essentially the recording of interferometric fringes on a photographic plate. In order to record accurately the phase and amplitude of the desired objects, it is necessary to maintain a high degree of vibrational stability. Otherwise, unwanted interference fringes might occur to obscure the desired image. The wavelength nature of light is extremely sensitive. Since a wavelength of light is so small (2.48×10^{-5} inches), the slightest movement will introduce undesired fringe patterns. Ever since the wave nature of light became generally accepted, interferometry has been the primary method for making measurements with extreme accuracy [3]. The extremely small wavelength of light, of the order of 5×10^{-5} cm, coupled with the fact that interferometric means are available for detecting changes of only a small fraction of this length indicate the degree of accuracy that can be achieved. Widespread applications of interferometry attest to its usefulness in engineering fields. For example, it is used for the testing of optical components, the optical gaging of machine tools, the study of air flow in wind tunnels, and the standardization of the fundamental units of length. Given the wide range of possibilities, it is clear that fundamental improvements or innovations in current techniques should find applications in the field of Naval Engineering.

The advent of the science of holography has widened the scope of interferometry to such a degree that it is hard to imagine that holographic interferometry will not be one of the standard engineering tools for years to come.

Conventional interferometry can be used to make measurements on highly polished surfaces of relatively simple shapes. However, holographic interferometry extends the range by allowing measurements to be made of three-dimensional surfaces. With holography, a roughly machined part now can be measured to optical tolerance. Furthermore, complex objects can be examined interferometrically from many different perspectives by using the three-dimensional hologram. A single hologram is equivalent to many observations with conventional interferometry. Another important aspect of holographic interferometry is that an object can be examined at different times creating a useful material history of the specimen. One is now able to detect with wavelength accuracy any changes undergone by an object over a period of time. This aspect has significant potential in the field of shipboard vibrational studies.

To understand the basic process of holographic interferometry, consider the hologram of an object wave $O(x)$ as shown in Figure 3. The object wave at the hologram is denoted by $O(x)$ and can be written in the form:

$$O(x) = O_o(x)\, e^{i\phi_o(x)} \tag{33}$$

where $O_o(x)$ is real amplitude distribution, and $\phi_o(x)$ is phase distribution. The reference beam at the hologram is expressed as

$$R(x) = R_o\, e^{ik\, x \sin \alpha_R} \tag{34}$$

where R_o is the amplitude of the reference wave at the hologram, and α_R is the off axis angle [3].

The transmitted holographic wave field consists of many waves traveling in several directions which are determined by the linear vibrations of x in the exponents. The irradiance distribution consists of a series of fringes. Fringes are equally spaced straight lines perpendicular to the plane of the figure. For a hologram the reference wave is also plane and incident on the recording medium at an angle to the object wave resulting in a series of fringes. The hologram appears in the form of diffraction gratings because of this series of alternately clear and opaque fringe display.

The author's study is concerned with the single exposure hologram interferometer of a diffusing or vibrating square aluminum plate.

3. Photographic Plate Requirements

Due to the fact that the two beams utilized to form the interference fringes arrive from different directions, forming the so-called offset angle, the fringe frequency recorded by the photographic emulsion is extremely high. When recording three dimensional scenes, additional increases in frequency occur. Plates or films with extremely high resolution are, therefore, required. In order to calculate the plate resolution which is required, the fringe frequency ν can be determined from the relation (4)

$$\nu \simeq [2 \sin (\theta/2)]/\lambda \qquad (35)$$

where θ is the offset angle and λ is the wavelength of the light source. For example, using the above equation, it can be determined that a hologram taken with a Helium-Neon laser (632.8 nm wavelength), with an offset angleof 45 degrees, requires a plate resolution in excess of 1200 lines per millimeter.

B. TECHNIQUES OF INTERFEROMETRIC HOLOGRAPHY

Since a hologram of an object records the phase and amplitude in the order of wavelengths, holographic techniques are extremely well suited to nondestructive testing. Interferometric holography permits the detection and measurement of minute changes in the surface shape of an object by providing a viable process for the comparison of each point on the surface with itself before and after a change takes place [5]. Because of extreme sensitivity to surface deformations, the technique can be used to gain meaningful information with regard to structural characteristics of a component by observing the surface movement produced when the object is subjected to a mild stressing force. As such, it offers the potential for many inspection problems wherein the defect of interest can be made manifest as an anomaly in an otherwise regular interferometric fringe pattern. The surface of a component under test can be mildly stressed in many ways, which include acoustic vibration, thermal excitation, pressurization, and simple mechanical force. Methods presented in this study utilize the acoustic vibration method of displacement. By combining holography with vibrational excitation techniques from an electronic shaker it is possible to record interferometrically the physical properties of relatively large surfaces as they are deformed by plate wave signatures at various frequencies. As a result, many problems heretofore not amenable to visible inspection are now open for investigation. Representative examples would include thickness variations of thin walled structures, the uniformity of bond strength, and the existence of disbonds in composite material structures. There are three different types of holograms which are particularly well suited to this use.

1. Real-Time Holography

The basic principles of real-time holography have been covered in this chapter part A, Section 2, pp. 18-21. This method consists of taking a single exposure of a static object. The hologram is then developed in its original position. Since it must remain within a fraction of a wavelength of its original position, developing tanks which allow in-space processing commonly are used for this type of holography. When reconstructed with the original reference and object beams, the holographic image will be superimposed on the original object. If the object is then displaced slightly, interference fringes can be observed at the instant that they occur - hence the name real-time holography. The outstanding advantage of this type of hologram is that numerous different kinds of movements can be studied with a single holographic exposure. Unfortunately, fringe contrast and sensitivity generally are reduced when using this technique to study vibratory motion. The time saving and flexibility which are provided by this method, however, generally outweigh these disadvantages.

2. Time-Average Holography

Time-average holography consists of taking a single exposure hologram of an object while it is undergoing cyclic vibratory motion. Due to the nature of vibratory motion, that is, the fact that an object subjected to this type of motion will spend the greatest percentage of time at its displacement extremes, a hologram will record interference fringes corresponding to the position of an object at its largest displacement, provided, of course, that the exposure time is long compared to one period of the vibration cycle. This technique is a

valuable tool in the study of one specific vibration mode of a test specimen. A time-average hologram permanently stores information about the amplitude of vibration and location of vibratory nodes.

3. Double-Exposure Holography

Double-exposure holography consists of taking an exposure of a specimen, displacing the object, and then exposing the same photographic plate once again to the specimen in a vibrating condition. When the hologram is processed and reconstructed, it will display the interference pattern caused by the displacement of the object which occurred between exposures. This is an excellent technique for studying objects which have undergone static loading such as beams or pressurized piping [6]. Double-exposure hologrpahy also is suitable for investigating mode shapes of plates such as portions of the hull of a ship as it undergoes vibrational stresses. In real-time holography continuous comparison of surface displacement relative to an initial state is considered by vibrating the subject plate at various frequencies. Since the purpose of this study is to establish the mode shape deviations caused in an aluminum plate clamped on all four sides, double-exposure holography becomes an excellent technique for recording the history of surface displacement over a fixed period of time (13). Each exposure is made with an identical reference wave, and this time-lapse method alleviated the problems encountered with registering reconstructed and original waves coincidentally. After the exposure of the hologram, the subject and optical components used to illuminate the specimen are no longer of concern. The desired comparison waves are reconstructed on the plate. The double-exposure holographic method is similar to real-time methods in most aspects. The

double-exposure interferogram requires making two holograms on a single recording medium. One of the two holograms yields a primary image that constitutes the comparison wave as in the single exposure real-time case. The test or displaced wave is not the object itself, but rather a reconstructed wave from the changed object. Therefore, an interference phenomenon, caused by changes in optical path through the object between exposures, is produced when the double-exposure hologram is illuminated for analysis and photographic reproduction [3].

III. EXPERIMENTAL PROCEDURE

A. HOLOGRAPHIC SYSTEM

The components of the holographic system used can be divided into three distinct groups: first, the holographic equipment utilized to produce holograms in general; second, the vibration equipment utilized for this specific investigation; and third, the photographic plates and their development system which enables in-place processing to be accomplished.

1. Holographic Components

The support for all of the optical components and the test specimens is a vibration isolation table which rests on four vibration isolation mounts located in the legs. The table, which has a honeycomb stainless steel top drilled and tapped with 1/4-20 mounting holes on one-inch centers, weighs approximately 1000 pounds. It floats on air bags which are pressurized with a regulated supply of nitrogen and which are installed in each leg. Automatic leveling is accomplished by regulators that control the nitrogen flow to each leg and respond to any excitation causing movement of the table. The table, with optical components in place, is pictures in Figure 4a. Figures 4b and 4c display the path of the reference beam from the Helium-Neon laser.

The optical components of the holographic system and their functions are listed and described below. Their position on the table is depicted schematically in Figure 5.

(1) LASER: A 10 milliwatt, Hughes model 3170H, Helium-Neon laser with a 5 millimeter beam was utilized. It provides the coherent and monochromatic light source.

(2) BEAM STEERER: A Jodon BA-500A Beam Steerer was utilized and is pictured in Figure 6a. It provides the horizontal and vertical beam steering capability necessary to direct the beam along the proper path after it leaves the laser.

(3) LASER SHUTTER: A Jodon S-10B Shutter was utilized. It provides photographic plate exposure control with shutter speeds variable from T to 125th of a second.

(4) VARIABLE BEAM SPLITTER: The Jodon VBA-200 Variable Beam Splitter utilized is pictured in Figure 6b. It provides a continuously variable beam splitting capability which splits the laser beam into the object and reference beams and enables fine adjustment of beam intensities at the photographic plate.

(5) MIRROR POSITIONERS: One of the three Jodon MH-50 Mirror Positioners used is pictured in Figure 6c. They provide a precise beam positioning capability and enable equal path lengths to be achieved.

(6) MIRROR MOUNT: A Jodon RM-45 Mirror Mount was utilized. It provides the same service as Mirror Positioners; however, it has no fine adjustment capability.

(7) LENS PINHOLE SPATIAL FILTERS: One of the two Jodon LPSF-100 Spatial Filters is pictured in Figure 6d. They remove irregularities in the beam due to imperfections or dirt on the beam splitter or mirrors. In addition, they expand the object and reference beams just prior to arrival at the object and photographic plate respectively. For the object beam, a pinhole size of 50 microns was used with a microscore objective of 20 x 0.40. For the reference beam, a pinhole size of 25 microns was used with a microscope objective of 20 x 0.40.

In addition to these components, a light meter was used to measure the respective intensities of the object and reference beams. It consisted of a planar diffused silicon PIN photodiode connected to a digital voltmeter. This device, used in conjunction with the variable beam splitter, enables the beam intensities to be matched accurately at the photographic plate.

2. Vibration Equipment

In order to provide the excitation required to displace the test specimen, a piezoelectric shaker was utilized. The shaker, which incorporates a PZT transducer to induce mechanical motion, was driven by an audio oscillator. Since the displacement of the shaker is directly proportional to the input voltage at the rate of 0.12 microns per 100 volts, the signal from the oscillator was stepped up through a power amplifier and transformer. A voltmeter was wired to the circuit in order to monitor the shaker voltage. This arrangement allowed a larger range of shaker displacements and enabled these displacements to be monitored easily. A digital frequency counter was connected to the oscillator to increase the accuracy of frequency read-outs. The shaker which was utilized, a JODON EV-30, is pictured in Figure 7. The drive and monitoring system for the piezoelectric shaker is pictured in Figure 8.

3. Photographic Plate and Development System

a. Photographic Plates

The photographic plates used were KODAK holographic plates specifically designed for use in holographic research. Designated 120-02, these are slow but clear when exposed with Helium-Neon lasers and meet the resolution requirement outlined in Chapter II. Successful results were obtained by using exposure times of 8-10 seconds.

b. Development System

The development system, pictured in Figures 9 and 10, consist of a holding tank to allow in-place processing, 5 aspirator bottles containing the processing fluids, and a network of tubing providing flow from the bottles to the tank. A valve manifold enables each chemical to be run into the tank, and a pump is used to provide necessary agitation. Following the stipulated rinsing times, chemicals are drained from the tank to bottles on the floor for re-use. Appendix A describes the operation of the valve manifold system.

B. TEST SPECIMEN SELECTION

Three questions must be answered before test specimens logically may be selected, namely: From what material should the specimens be made? What shape should they be? What size should they be?

1. Material Selection

The selection of the specified material for use as test specimens was made with consideration being given to two primary requirements. The material chosen should be a metal commonly used for Naval applications and should have a low damping capacity.

In order to understand better the damping requirement, consider that an excited metal plate vibrates in much the same way as a mass-spring-damper system in parallel. The greater the damping inherent in the plate material, the greater the width of the resonant peak in the response curve. Figure 11 displays graphically the difference in response curves for typical high and low damped systems.

The resonant frequency in each case occurs at the response peak. In order to observe a resonant frequency shift due to a cut in the plates, a minimum peak width is highly desirable. If f_d is the width

of the resonant frequency peak and f_c is the change in resonant frequency due to a cut, the f_c must be much larger than f_d in order to be able to isolate a frequency change due to the cut. Once the requirements for a low damped material were established, a method of quantifying material damping was sought.

One commonly used method of measuring the damping capability of a material is the specific damping capacity (SDC) [7]. This measure is derived from the decay of free oscillation of an excited bar specimen as shown in Figure 12. The SDC is then calculated from

$$SDC = \frac{(A_n - A_{n+1})^2}{A_n^2} \times 100\% \qquad (36)$$

This relationship, which directly relates absorbed energy to the square of the amplitude, enables materials to be tabulated according to their damping capabilities. Table I lists some common structural materials and their SDC's.

Based on the two requirements stipulated above for this investigation, aluminum alloy 2024-T4 was chosen as the test specimen material.

2. Specimen Shape

In order to be able to conduct the investigation with the best possible chance for meaningful results, a shape must be chosen for which there exists ample theoretical information. In addition, the physical application of boundary conditions must be realistically feasible on the shape chosen. An all-sides-clamped configuration was chosen to satisfy the latter of these two requirements. This decision ensures that the greatest possible accuracy will be obtained while

physically satisfying the boundary conditions in the laboratory. Three shapes were then considered for the plates: circular, square, and rectangular.

Considerable theoretical information on the vibration of circular plates can befound in reference [8]. However, the complications involved with constructing a specimen mount made this choice undesirable [2].

As noted by Hoffman [2], a square plate at first appeared to be an excellent choice; however, further research exposed an interesting phenomenon which occurs in the case of a vibrating square plate. This condition, called degeneracy, occurs when the allowed frequencies become equal in pairs due to the equal length of sides. When the degeneracy occurs, an infinite number of mode shapes may appear at the same frequency. In order to avoid the frustration of coping with this condition, the square plate also was rejected.

Rectangular plates were then considered for the test specimens. These ultimately were chosen for several reasons. They lend themselves well to laboratory mounting. Furthermore, extensive theoretical information on vibrating rectangular plates is available [8], and special complications are not involved in isolating a specific resonant frequency or mode shape.

3. Specimen Size

The exact size of the plate was chosen carefully with consideration being given to three specific constraints. First, the area of the plate required compatibility with the capability of the available holographic equipment. Second, the length of the sides was constrained further by the fact that the available tabular data on frequency parameters

were limited to specific side length ratios. Third, the thickness was also an important decision because it figures prominently in the calculation of flexural rigidity which is a major contributor in the theoretical determination of fundamental frequencies. Bearing each of these constraints in mind, a rectangular plate 6 x 4 inches on the sides, with a thickness of 0.020 inch was chosen. One of the plates used is shown in Figure 13.

Also, the geometry described allows one to use the data listed in reference [8] for a clamped-clamped-clamped-clamped (C-C-C-C) plate for theoretical analysis.

C. THEORETICAL FREQUENCY DETERMINATION

Once the material, shape and exact size of the test specimens had been selected, calculations were made to determine the expected frequencies for each of the mode shapes [2]. The frequency parameters, f_n, for an all-sides-clamped rectangular plate are given as

$$f_n = \omega_n b^2 \sqrt{\rho/D} \tag{37}$$

where

ω_n = circular frequency of the n^{th} mode in radians/second

b = length of shorter side in feet

ρ = density in slugs/foot squared

D = flexural rigidity in foot-pounds

n = number of mode

The flexural rigidity is defined as

$$D = \frac{Eh^3}{12(1 - \nu^2)} \tag{38}$$

where

E = Young's modulus in psi

h = plate thickness in inches

ν = Poisson's Ratio

For the aluminum alloy 2024-T4 plates which were used, values of the physical constants are:

$E = 10^7$ psi

$\nu = 0.33$

$h = 0.020$ inches

$b = 4.00$ inches

This gives a flexural rigidity of

$D = 0.6234$ ft-lbf

Further, for an aluminum alloy 2024 plate 0.020 inches thick

$\rho = 0.008723$ slugs/ft^2

Therefore

$$\sqrt{\rho/D} = 0.11828 \text{ sec/ft}^2$$

Then for a rectangular plate with a side length ratio of 1.5, the frequency parameters, f_n, are [8]:

m	n	fm,n
1	1	27.01
2	1	65.50
1	2	41.72
2	2	79.81

The mechanical properties of aluminum alloy 2024 are:

Cu = 1.6%

Mg = 2.5%

ZN = 5.6%

Cr = 0.3%

Ultimate tensile strength = 82,000 psi

Endurance limit = 24,000 psi

The fundamental frequencies were calculated to be:

$\omega_{1,1}$ = 327.0 HZ

$\omega_{2,1}$ = 794.8 HZ

$\omega_{1,2}$ = 506.2 HZ

$\omega_{2,2}$ = 968.45 HZ

D. TEST SPECIMEN MOUNT

In order to support the aluminum plates in such a way as to permit testing in accordance with the experimental methods, a suitable mount was designed and built. Due to the nature of the experiment, several factors had to be taken into account during the design phase.

1. Boundary Conditions

Since test specimen selection and subsequent theoretical frequency calculations were based on a rectangular plate clamped on all sides, care was taken to assure that this boundary condition was satisfied to the fullest degree possible.

2. Shaker Mount

Since exact frequencies were to be measured, the piezoelectric shaker was mounted securly to eliminate inaccuracies inherent with shaker movement. A pair of braces were connected between the shaker and the specimen frame to ensure complete system stability.

3. Table Isolation

Due to the nature of holography and the importance of table stability, as outlined in Chapter II, the mount was constructed in such a way that vibration was not transmitted to the holographic table. The specimen mount designed and built to meet these specifications is shown in Figure 7.

E. TEST PROCEDURE

1. Making a Hologram

a. Preparing for Exposure

In order to arrange the equipment to make a good hologram, the following steps must be taken. To begin, the optical components and object must be aligned so that the path lengths of the reference and object beams are nearly equal. This will ensure that the temporal coherence length provided by the laser will be enough to result in high-contrast interference fringes. In practice, these lengths were adjusted within an inch of each other. Once this has been accomplished, the nitrogen support bed table should be activated to provide the necessary vibration isolation. Now, the laser should be turned on to allow the optical components to be aligned so that the two beams are illuminating the object and the plate. The beam splitter is then adjusted until the intensities of the respective beams are essentially equal. Although beam equal intensity is desired, this property was not found to be a

necessity to produce useful holograms. For Kodak 120-02 holographic plates, the shutter is operated in the non-automatic mode to allow double exposure timesof 3.5 seconds static and 5.0 seconds dynamic with a combined photovoltaic intensity of approximately .070 volts.

b. Exposing the Plate

After the previously described alignment procedures have been followed, the holographic plate is ready to be exposed; with the laser beam covered and with the room in total darkness, the plate may be removed from its box and carefully placed in the holding/developing tank. Then the plate box must be recovered carefully to avoid exposing any other plates. The laser power supply was not secured when placing the plate in the developing tank because a small warmup time was required for the laser beam. Shadowing the beam at its output end with a black cloth achieved the desired results of maintaining total darkness. For best results a photographic developing timer was used to ensure that the desired exposure times were achieved. Next, the laser beam was uncovered, the shutter opened, and the timer energized. This process is conducted separately for both the static and dynamic exposure durations. These steps must be executed smartly and carefully to protect the plate from any excess laser radiation exposure to prevent jolting inadvertently the isolation table. Once the plate has been exposed, the light-tight cover is placed over the developing tank. When this has been accomplished, the room lights may be turned back on. It is noteworthy that if stray beams are generated in either the object or the reference plane, multiple holograms will be produced. The author discovered this phenomenon inadvertently by producing a hologram with three exact images visible at different angles separately and as a group.

The cause was determined by reconstructing the system and looking through the developing tank for stray beams. Stray beams of moderate intensity were noted in the area of the beam splitter and the respective spatial filters. The problem was rectified easily by shielding these undesired beams with black objects so that the holographic plate was exposed only to the reference and object beams of the laser.

c. Developing the Plate

After the exposure, the processing of the 120-02 holographic plate must be performed in the following manner, as recommended by KODAK. For manifold operations, follow the procedures outlined in Appendix A and depicted in Figure A-1.

(1) Open valve No. 2 allowing the D-19 developing solution to fill the tank. As soon as this valve is opened, begin a 7 minute timer. When the tank is filled, close the valve and turn on the pump to agitate the tank's contents. When seven minutes time has passed, open the drain valve and secure the pump. Operate the pump at 3/4 speed.

(2) Open valve No. 3 allowing the tank to fill with KODAK INDICATOR STOP BATH. When 15 seconds have passed, open the drain valve and secure the pump. Operate the pump at full speed.

(3) Open valve No.4 allowing the KODAL FIXER to fill the tank. Start a 7 minute timer when the valve is opened. Once again, pump at full speed. Secure the pump and drain the tank at the end of 7 minutes time.

(4) Repeat step 3 with distilled water via valve No. 1.

(5) Repeat step 3 with one part methanol and one part water via valve No. 5. This rinse is required to remove a high level of residual

sensitizing dye from the emulsion. This dye is distinctly blue, and experience may dictate a lesser rinse time for the removal of this color. As a substitute for the methanol solution, two parts ethanol and one part water also may be used.

(6) Finally, wash in distilled water again for a period of 6 minutes as noted in step 4.

When the final wash has been completed, the hologram should be allowed to air dry in place. After drying is complete, the hologram is ready to be reconstructed.

d. Reconstructing the Hologram

In order to reconstruct a time-average or double-exposure hologram, the original reference beam alone must be shined on the plate. Then, by looking through the hologram in the direction of the original object, the reconstruction of the object will be clearly visible. Any fringes which are visible due to the displacement of the object are a permanent part of the hologram, so it is not necessary to maintain the photographic plate in its exact position for reconstruction. The intensity of the reference beam may be adjusted to vary the brightness of the reconstructed image.

The reconstructed image may then be photographed to obtain a permanent record which can be viewed or studied without the aid of the laser. Any high speed film can be used to accomplish this; however, three films in particular are excellent for use with red-emitting lasers. Kodak Technical Pan SO-115 is a 35 mm film manufactured specifically for use in holographic reconstruction. Polaroid 57 high speed and Kodak 55 Pos/Neg films are good reconstruction film, but they are not as clear as the Kodak SO-115 film. Appendix B discusses the

Polaroid Photographic System alignment to be used for documenting expeditious results of the double-exposure hologram and for real-time holography. In cases where time is not a constraint, utilization of 35 mm photographic procedures generates more vivid pictures of the holograms.

In the case of real-time holography, the process is somewhat different. Once again the reference beam alone will produce a reconstructed image of the object. In order to observe a real-time hologram, the original object beam also must be activated. Then provided that the plate and object are in exactly their original positions, the reconstructed image will appear superimposed on the actual object as desired. The beam splitter should be adjusted so that the object and its reconstructed image appear in equal intensity. When that has been accomplished, excitation of the object will cause the real-time fringes which may be seen viewing the object through the hologram. During excitation, the fringes are visible, and the reconstruction may be photographed.

Unfortunately, the author's numerous experiments in real-time holography failed due to small movements of the photographic plate, and it was necessary to employ double-exposure holography. Movement was ascertained by viewing the real-time hologram after it has been developed and before the piezoelectric shaker was energized by observing numerous fringes while the unit was in a static condition. As a result of these small movements, the major advantage of real-time holography, namely, the recording of the entire spectrum of mode shapes initiated by thier respective resonant frequencies on a single hologram, was lost. However, the advantages of double-exposure holography are significant

because of the time history results imprinted on the plate. The major disadvantage of this method is the overall time required to run separate hologramsto record the desired resonance fringes.

2. Holographic Techniques Utilized

a. Initial Attempts

Numerous initial experiments were conducted utilizing real-time procedures but slight plate movement hindered the final results because of the fringes noted before the electronic shaker was activated. Modifications were made to both the plate developing tank mount and the specimen plate/shaker mount assemblies to correct for the infinitesimal movement noted. It finally was determined that the spring clamp assemblies inside the developing tank which secure the Kodak 120-02 Holographic Plate were not firmly securing the plates. Since major modifications to the developing tank holding clamps would be required, a decision was made to abandon real-time procedures and to utilize the double exposure methods.

The procedures required to generate a hologram are not as fool proof as the author may have inferred. At the outset of this study, numerous failures were recorded in attempting to make a hologram of a model ship. Beam angles were modified, chemicals were changed, and laser beam intensities were varied to no avail. It finally was ascertained that the photographic plates being used were defective. On the first attempt with a new Kodak 120-02 holographic plate, a successful hologram was recorded of a model destroyer as shown in Figure 14. To gain proficiency in the holographic procedures, the author made many holograms of the model ship, and one also of a gear system (Figure 15) and a bolt in a plate (Figure 16).

As noted by Hoffman [2] and verified by the author, three tests should be conducted on the hologram prior to full development. If the plate fails any of these tests, it is not a usable hologram, and the remainder of the processing may be discontinued. The first test is carried out just after completion of the fixing process. When the Kodak Fixer has been drained from the developing tank and replaced with distilled water, the light tight cover may be removed. Once this has been accomplished, the photographic plate should be observed. It should be light blue in color and clear enough to see through. If the plate is too dense to see through with the room lights turned on, then it will not be a useful hologram. The second test may be given after the initial water wash has been drained from the tank. With the reference beam illuminating the plate, one should be able to observe faintly the holographic image on the photographic plate. The third test may be given after the final water wash has been drained from the tank. With the reference beam turned on, the plate should be viewed in the direction of the oncoming beam. As a result of diffraction, several red dots in a horizontal line should be evident. If there is only one red dot, the plate is not a hologram and need not be dried.

Once the ability to make useful holograms was mastered, an unflawed 0.020 inch Aluminum 2024-T4 rectangular plate was bolted into its housing frame to create a clamped-clamped-clamped-clamped (C-C-C-C) assembly for vibration analysis. At this juncture it was first noted that the plate was re-orienting inside the film holder causing a fringe pattern prior to activating the electronic shaker. At first, movement of the plate was suspected; therefore, a 0.040 inch thick aluminum 7078 plate was clamped into the housing, and real-time holograms were

attempted. The same static fringes were noted which substantiated the fact that movement was occurring in the development tank holder. Experimental observations of the plate at various frequencies also showed that the piezoelectric shaker did not generate enough power to drive the 0.040 inch plate through a full spectrum of resonance mode shapes. Although the shaker is designed to run at a maximum of 2000 volts peak-peak, available transformers could generate approximately 1200 volts peak-peak at maximum. At this point a decision was made to return to the 0.020 inch aluminum 2024 plate for the analysis using double-exposure holographic techniques. A single exposure hologram of the aluminum 2024 plate prior to analysis is shown in Figure 17.

b. Pre-Flaw Holograms:

After the aforementioned problems had been resolved, double-exposure holograms of the test plate were made. Calculations were made using the data compiled by Liessa to determine theoretical resonant frequencies [8]. Double-exposure holograms were made at these theoretical frequencies to observe the results. As noted by Figure 18, the desired fundamental mode shape was not observed. This was attributed to the coat of paint on the plate or some unknown defects in the material composition of the plate, since calibration of the electronics equipment was considered accurate. Double-exposure holograms were then run at the fundamental and subsequent modes and recorded as shown in Figures 19, 20 and 21.

c. Post-Flaw Holograms

A 1-inch through-thickness vertical slit was placed in the aluminum 2024-T4 plate. Double-exposure holograms were run at the

various resonant frequencies which could be detected readily. As expected, the recorded mode shape frequencies of the flawed plates were not the same as the nonflawed plates. The signal generator was adjusted to accent the noted resonances, and then a hologram was generated. The results of this endeavor are pictured in Figures 22, 23, 24, 25 and 26.

IV. EXPERIMENTAL RESULTS

A. THEORETICAL BASIS

1. Methods in Vibration Analysis

In the fields of both theoretical and applied engineering and physics, extensive research is in progress to answer the questions regarding the analysis of fringe motions generated by vibration as depicted in a hologram. One such study has been in progress by Tonin and Bies [9].

Modern procedures for obtaining time-averaged holograms are common. However, deciphering holograms of complex vibrations is very difficult because one must first assume the motion before analysis can proceed. Characteristic functions for periodic non-sinusoidal vibration at a single frequency have been evaluated by several research works [2 to 8]. Characteristic functions also have been derived for vibration simultaneously in modes at two different frequencies.

Tonin and Bies [15] have shown that the fringe motion for rectilinear motion at an angle $\tan^{-1}(\frac{b}{a})$ to the normal surface pictured in Figure 27 is:

$$\frac{\Omega}{k} = a(\cos\theta_1 + \cos\theta_2) + b(\sin\theta_1 - \sin\theta_2) \qquad (39)$$

where

Ω is the argument of characteristic fringe function $J_o(\Omega)$

k is the wave number

θ_1 is angle of illumination vector to the relative normal of observed surface

θ_2 is angle of observation vector relative to the normal to the observed surface

a is amplitude of normal component of assumed sinusoidal motion

b is amplitude of tangential components of assumed sinusoidal motion

The motion of the surface is assumed to lie in the plane of the illumination and observation vectors as illustrated in Figure 30 where a right-handed coordinate system is assumed. Each point $\underline{i}$ of a reconstructed time-arranged hologram has a characteristic set of values Ω^i, $\theta_1{}^i$, and $\theta_2{}^i$. However, as the two components $\underline{a}$ and $\underline{b}$ are to be determined using $\frac{\Omega}{k}\ a(\cos\theta_1 + \cos\theta_2)\ + b(\sin\theta_1 - \sin\theta_2)$ two separate time-averaged holograms are required with different directions of illumination and observation. A principal problem is that Ω^i can be determined only with confidence at the centers of fringes, and two fringe centers are not likely to occur at the same spot on the surface. Hence interpolation of Ω^i is generally required. However, according to Tuschak and Allaire [10], interpolation has been shown to generate gross errors; thus an alternative procedure will be used. The intersection of the latter plane and the vibrating surface defines a line of observation in the surface alone which the components of motion tangential and normal to the line and in the plane may be determined.

Tonin and Bies characterize position along the line of observation by a length coordinate ξ and suppose that the tangential and normal components of motion along the line may be represented as analytic functions of ξ [9]. The functions $a(\xi)$ and $b(\xi)$ are expressed as finite trigonometric series:

$$a(\xi) = \sum_{n=N_1}^{N_2} [x_n \sin(n\xi) + y_n \cos(n\xi)]$$

$$b(\xi) = \sum_{n=N_1}^{N_2} [w_n \sin(n\xi) + z_n \cos(n\xi)] \qquad (40)$$

The quantities x_n, y_n, w_n and z_n are assumed n^{th} order vibration component amplitudes of the surface motion. The bounds N_1 and N_2 are the least and greatest order numbers considered in the analysis.

The intersections of the line of observation in the surface and the dark fringes on the reconstructed image determine a set of z points with values Ω^i, ${\theta_1}^i$, and ${\theta_2}^i$. Use of eqn (39) allows the writing of the following system of equations:

$$\begin{aligned} a_1c_1 + b_1S_1 &= R_1 \\ a_2c_2 + b_2S_2 &= R_2 \\ &\vdots \\ a_nc_n + b_nS_n &= R_n \end{aligned} \qquad (41)$$

where

$$c_i = \cos{\theta_1}^i + \cos{\theta_2}^i \qquad (42)$$

$$S_i = \sin{\theta_1}^i + \sin{\theta_2}^i \qquad (43)$$

$$R_i = \frac{\Omega^i}{k}$$

Substitution of eqn. (40) into eqn. (41) yields

$$\sum_{n=N_1}^{N_2} x_n \sin(n\xi_i)c_i + \sum_{n=N_1}^{N_2} y_n \cos(n\xi_i)c_i + \sum_{n=N_1}^{N_2} w_n \sin(n\xi_i)S_i$$

$$+ \sum_{n=N_1}^{N_2} z_n \cos(n\xi_i)S_i = R_i \quad \text{for } i=1,2,3,\ldots,n$$

where ξ_i, c_i, S_i and R_i are determined from the time-averaged holograms.

Another system for analyzing holograms was undertaken at the David W. Taylor Naval Ship Research and Development Center in Bethesda, Maryland, by Sikora [11]. Sikora's hypothesis is that several authors have proposed methods to derive the general displacement field from a double-exposure hologram but that these methods have often been cumbersome to apply because they have relied upon measuring fringe locations in space, knowing detailed coordinates on the surface of the object, or taking a large number of fringe readings to solve over-determined sets of equations. Simpler methods also have been proposed for such cases as out-of-plane deformations, pure bending, simple shapes, etc. Sikora developed a series of three equations which relates the general displacement field obtained from usual and image-plane holograms of objects illuminated by collimated or point light sources. To accomplish this, he defined a coordinate system for the holographic plate requiring that the object be several plate distances away from the plate with system simplifications such that the system of equations can be made to decouple the displacement components.

2. Aluminum Plate Analysis

Since the purpose of this study has been to ascertain the applicability of holographic interferometry to nondestructive testing for shipboard systems, the aluminum 2024 plate in the flawed and nonflawed state is analyzed. Figures 19 through 26 represent the nonflawed and flawed holograms of the subject specimen plates. The basic equations for the development of fringe analysis to ascertain the beam deflections of the plates at various resonant frequencies are applied easily for a systematic study of the specimen. Fringe analysis is the key aspect to vibration analysis in holography. The location of the position of a dark fringe on a vibrating plate is determined by the relation

$$\phi = \frac{2n-1}{2} = y\frac{(\cos\alpha + \cos\beta)}{\lambda} \qquad (46)$$

where

ϕ is the location number of the dark fringe

n is the number of the fringe from the plates fixed boundary condition

y is the deflection of the plate

λ is the wavelength of the Helium-Neon laser (2.48×10^{-5} in.)

α is the angle of the object beam to the plate

β is the angle of the reference beam to the plate

Studies were conducted for the following mode numbers for a rectangular plate where m is the number of modes symmetric about the y axis and n the number of modes symmetric about the x axis:

(a) m = 1 n = 1

(b) m = 1 n = 2

(c) m = 2 n = 1

The object has been to compare experimental results to theoretical results in order to ascertain overall applicability of the method to Naval Engineering problems. Data points were generated for deflection versus fringe location on the vibrating plates as a function of the resonant frequencies and reference and object angles. Figures 28, 29, and 30 show the flawed versus nonflawed deflection patterns for the mode shapes: m = 1, n = 1; m = 1, n = 2.

B. PRE-FLAW CONDITIONS

Utilization of the procedures of double-exposure holography as the basis for analysis yielded excellent results for the mode shapes at various frequencies. Although frustration, trial, and error were time inhibiting factors, the end results substantiate the value of double-exposure holography as a permanent record to be employed in the science of holographic vibration analysis. Resonant mode shapes were noted at 324 HZ for the fundamental; 792 HZ for m = 2, n = 1; and 578 HZ for m = 1, n = 2 condition as listed in Table II. Figure 19 depicts the fundamental mode shape with very light resolution. The light resolution and scarcity of fringes were repeated on several experiments which led the author to conclude that the electronic drive system generates a fairly weak signal at low frequencies impairing ideal experimental results. However, Figures 20 and 21 display the results of the desired mode shapes at higher frequencies. Deflection curves generated at the subject mode shapes (Figures 28, 29, and 30) are consistent with

previously ascertained experimental results with the following points of interest. The lack of perfect symmetry in the nonflaw conditions is considered due to a small error in the object light beam setup. At the fundamental frequency, m = 1 and n = 1, the scarcity of fringes is attributed to the electronic drive system. At first the author believed that the lack of fringes was due to incorrect recording of the resonance condition. However, repeated experiments ascertained that the fundamental harmonics as shown in Figures 19 and 22 for the nonflawed and flawed conditions are correct.

Difficulties encountered in gaining perfect symmetry in the m = 1, n = 2 case were attributed to the location of the piezoelectric shakers drive bolt which hits the center of the aluminum plate. Also the angle at which one views the recorded hologram will give the appearance of slight deviation of the fringe pattern. Best results were achieved when the reference and object beams illuminated the plate at equal angles. The inspection angle by which one viewed the plate affected the symmetrical appearance of the m = 1, n = 2 mode.

C. POST-FLAW CONDITIONS

The aluminum 2024-T4 test plate was flawed with a through-thickness slit 1 inch long and 1/16 inch wide, and the specimen was vibrated again in order to generate characteristic mode shapes to compare the plate in an nonflawed condition. A very interesting condition is that the frequency shift from the flawed versus the nonflawed plate was not consistent. As shown in Table II, the fundamental mode is noted at 342 HZ, Figure 22. At 772 HZ the m = 2, n = 1 mode is intercepted, Figure 23; and at both 462 HZ and 532 HZ, the m = 1, n = 2 mode is evidenced in Figures 24 and 25. The author expected the mode shape

resonant frequencies to shift consistently downward, but only the m = 2, n = 1 case gave this result. As depicted in Table II, two resonances were recorded at m = 1, n = 2. At 468 HZ the nonflawed side of the plate, Figure 23, is in resonance while at 532 HZ, Figure 25, the flawed area of the plate is in resonance. Also recorded in the flawed plate study was the harmonic at the m = 2, n = 2 mode shape which generated the expected fringe pattern as shown in Figure 26. As previously noted, the deflection relationships between the nonflawed and the flawed plate conditions are shown in Figures 28, 29, and 30.

D. EVALUATION OF RESULTS

1. Measured Versus Theoretical

Comparison between the theoretical and experimental resonant frequencies was favorable for the specimen of a completely clamped rectangular aluminum 2024-T4 plate as shown in Table II. Although great care was taken to ensure that all associated reference and object beams were symmetrical, slight asymmetric conditions prevailed in the tests conducted under nonflawed conditions. Utilization of Liessa's plate theory relationships coupled with the experimental results listed in Table II shows that the experimental method followed is consistent for plate vibration analysis [8].

2. Pre-Flaw Versus Post-Flaw

As previously stated, no firm resolution could be made on the effect of the resonant frequencies concerning flawed versus nonflawed plates. Studies by Hoffman firmly ascertained that the resonant frequency for a flawed plate would be lower than for a nonflawed plate; however, the specimen used in his treatise was clamped on all four sides and in the middle (2). In the author's studies only, the m = 2, n = 1 mode

had a drop in frequency for the flawed plate of approximately 15 per cent. The other mode shapes showed an increase in resonance of approximately 10 per cent. Of course, a small amount of error could have been introduced by double-exposure holography. Each case studied shows a noticeable change in the mode shape between the flawed and normal conditions with a shift of the fringe pattern toward the flaw as depicted by Figures 19-25. The graphs of the associated mode shapes in Figures 28, 29, and 30 point out deflection differences presenting firm evidence of the flaws.

V. CONCLUSIONS AND RECOMMENDATIONS

A. CONCLUSIONS

The following conclusions can be ascertained from the results of the double-exposure hologram plate vibration study:

(1) Flaws in the rectangular plate clamped on all four sides generate resonant frequency shifts allowing one to analyze deflection patterns due to the flaw.

(2) Double-exposure holographic methods provide the analyst with a time-generated historic record of the mode shapes at the various frequencies.

(3) Double-exposure holography does not allow the study of the entire frequency spectrum in real-time conditions. This limitation may give rise to possible error in resonant frequency determination because one must rely on the human ear to depict resonant frequencies.

(4) Mode shapes in flawed plates show a shift in the mode shape.

(5) Holographic procedures are very sensitive to extraneous effects (e.g., temperature and movement of the plate holder).

These conclusions and the author's experiences in this study indicate that holograpahic procedures are viable tools for vibration analysis. However, because of the sensitivity required, the slightest deviation from procedure may result in failure. Certainly this science is in an embryo state as evidenced by the overall sensitivity of the equipment available.

If the available equipment can be improved, Holographic Nondestructive Testing (HNDT) will become a reality for a shipboard maintenance. However, equipment sufficiently durable and accurate to survive the conditions aboard a ship at sea is required if this procedure is to be used at sea. The acute definition of flaws obtained with this procedure makes HNDT a possible method for studying the conditions of piping systems, boilers, turbines, and pump casings on all ships, as well as another means of aircraft engine inspection for Aircraft Intermediate Maintenance Department personnel on aircraft carriers. Of course, the resonant frequencies and mode shapes of the system under normal operating (unflawed) conditions must be known as bench marks for follow-on analysis in comparing future conditions.

Currently, this system is not portable enough to be utilized successfully outside a laboratory environment. The accuracy, solid foundations, and complex operational procedures presently required preclude the use of this method aboard ship. However, if these difficulties are overcome, HNDT is a viable option to consider.

B. RECOMMENDATIONS

The potential use of HNDT and associated vibration analysis aboard ship requires further study in this field. Some recommended studies are the following:

(1) Since the plate holder experiences minute movements in the real-time holography development procedure, a method of developing tank isolation and an improvement on the plate clamps appear in order.

(2) Future studies in this science should begin with double-exposure procedures and then follow-on with real-time analysis.

(3) Procurement or development of the required electronic equipment to drive the electronic shaker to its maximum voltage is necessary for future studies of thicker plates.

(4) Conduct studies of elliptical plates, cantilever beam type assemblies, and other rectangular plates of various materials and thicknesses.

(5) Conduct a study on vibrating turbine blade with the goal of determining its application to shipboard use.

(6) Conduct a finite element computer study of the experiment on the flawed plate done in this treatise to compare the computed mode shapes at various frequencies to the measured mode shapes.

(7) Another topic of interest would be the generation of double-exposure holograms of heated plates to study the mode shapes due to different thermal gradients.

Since this is a relatively new science, the potential for growth is constrained only by the intensity of the analysts' inquisitiveness. Further studies are considered a must, and they are assumed to be very enlightening and positive contributors to modern science.

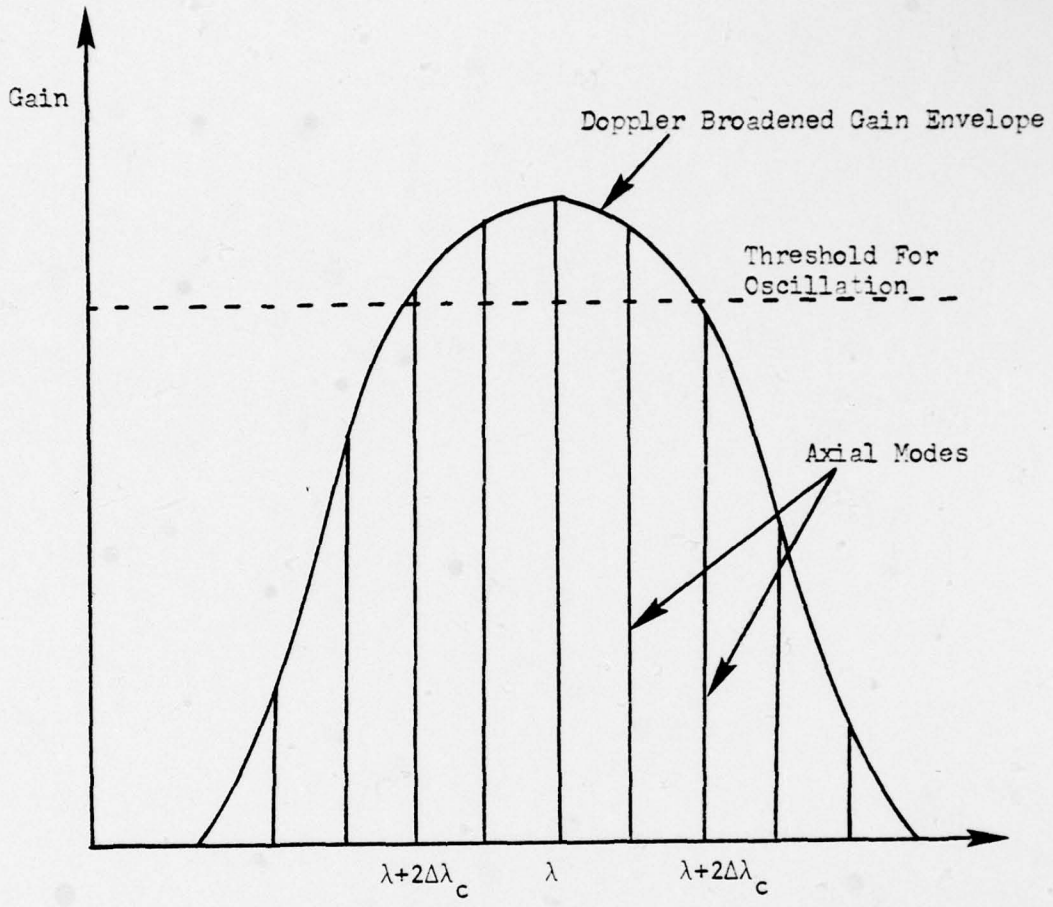

Figure 1. Typical Gas Laser Spectrum

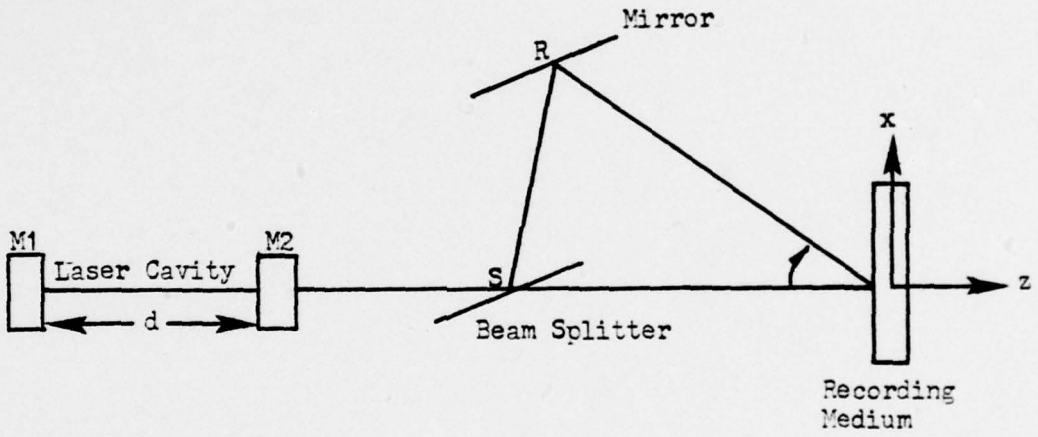

Figure 2. Two-Beam Holographic Laser Scheme

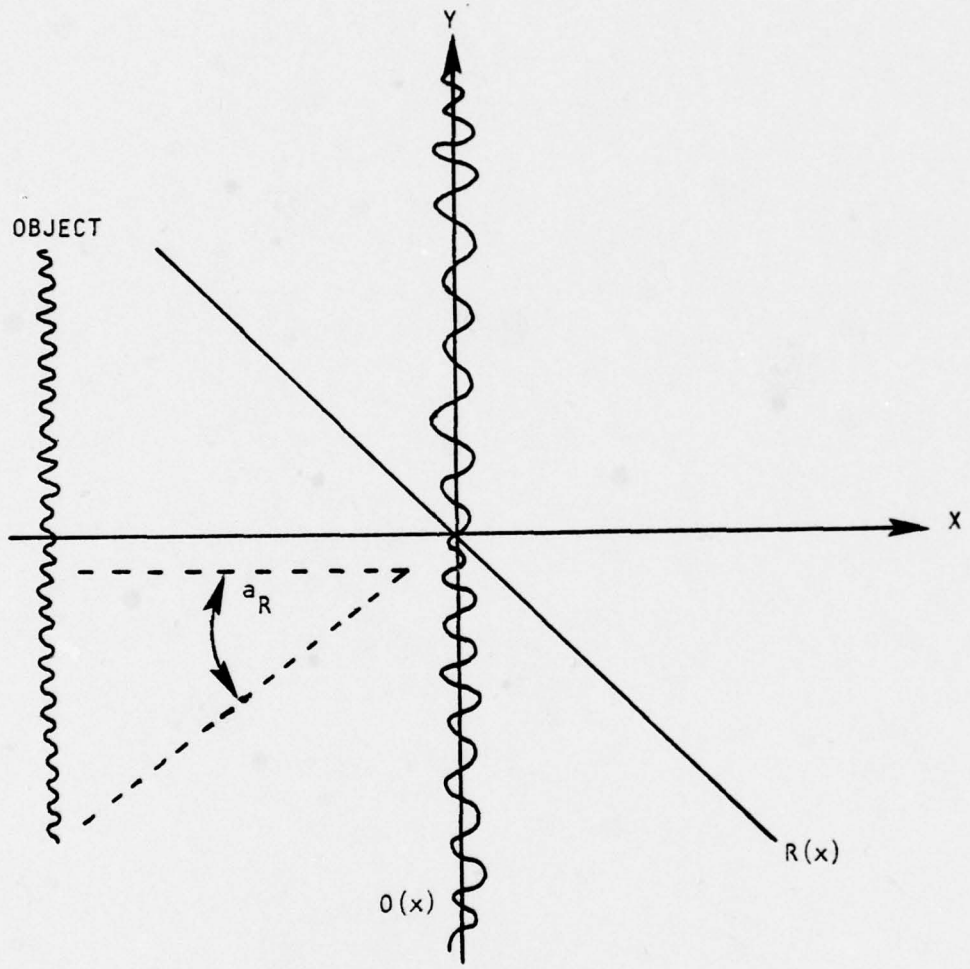

Figure 3. Object Wave Recording

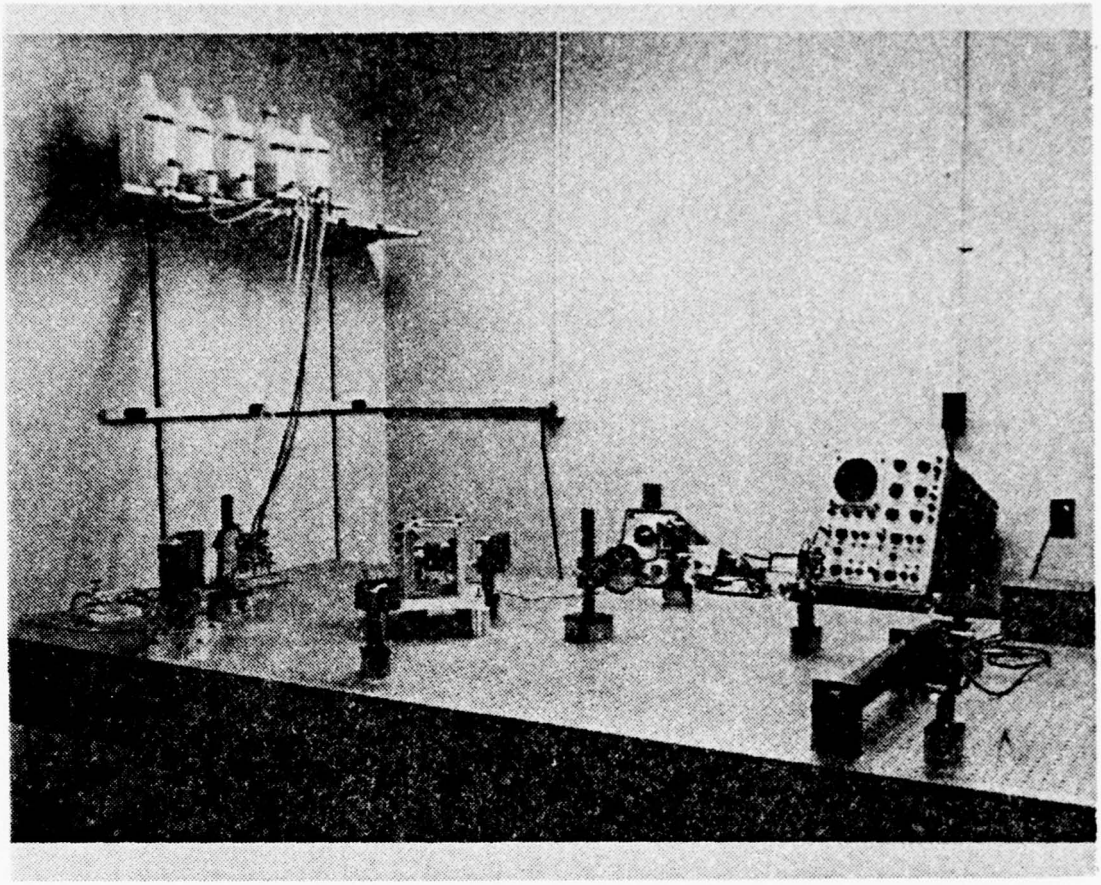

a) Holographic System with Laser Beam Turned OFF

Figure 4. Vibration Isolation Table with Laser, Optical Components, and Test Specimen in Place

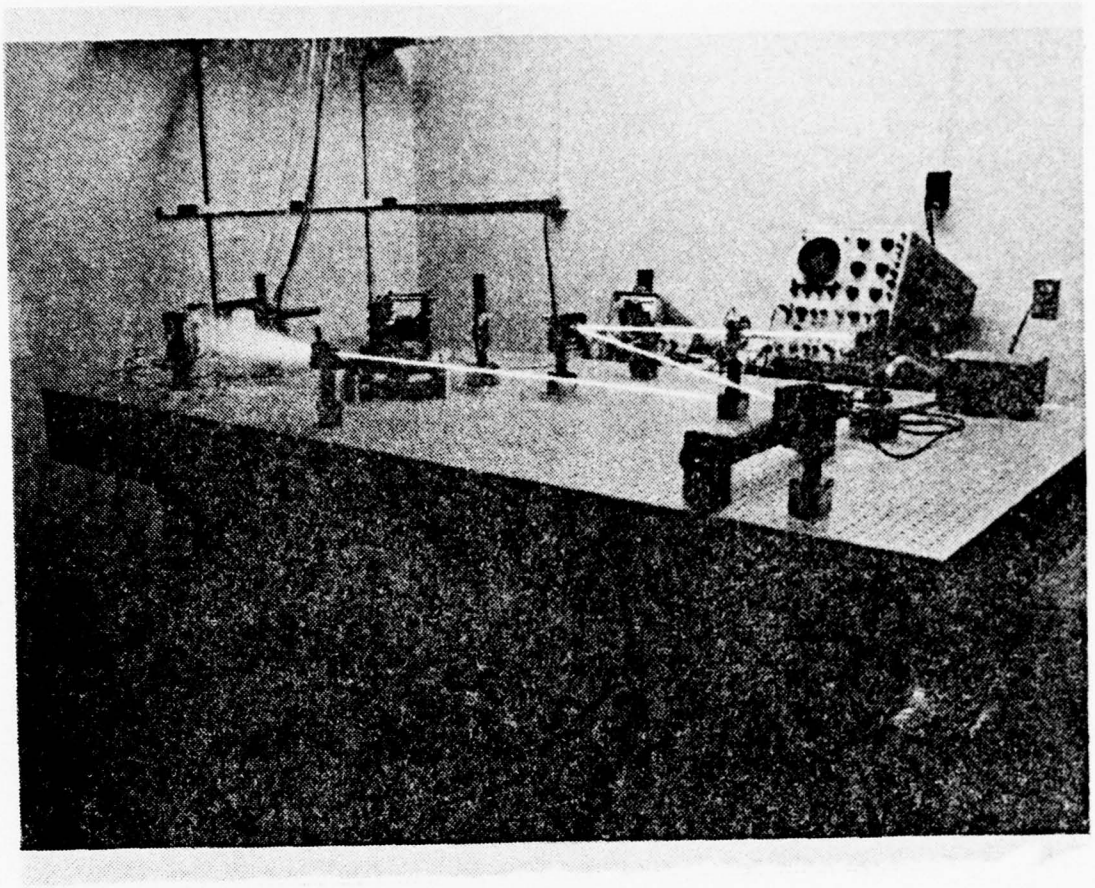

b) Holographic System with Laser Illuminating the Reference Beam in a Lighted Room

Figure 4. Vibration Isolation Table with Laser, Optical Components, and Test Specimen in Place

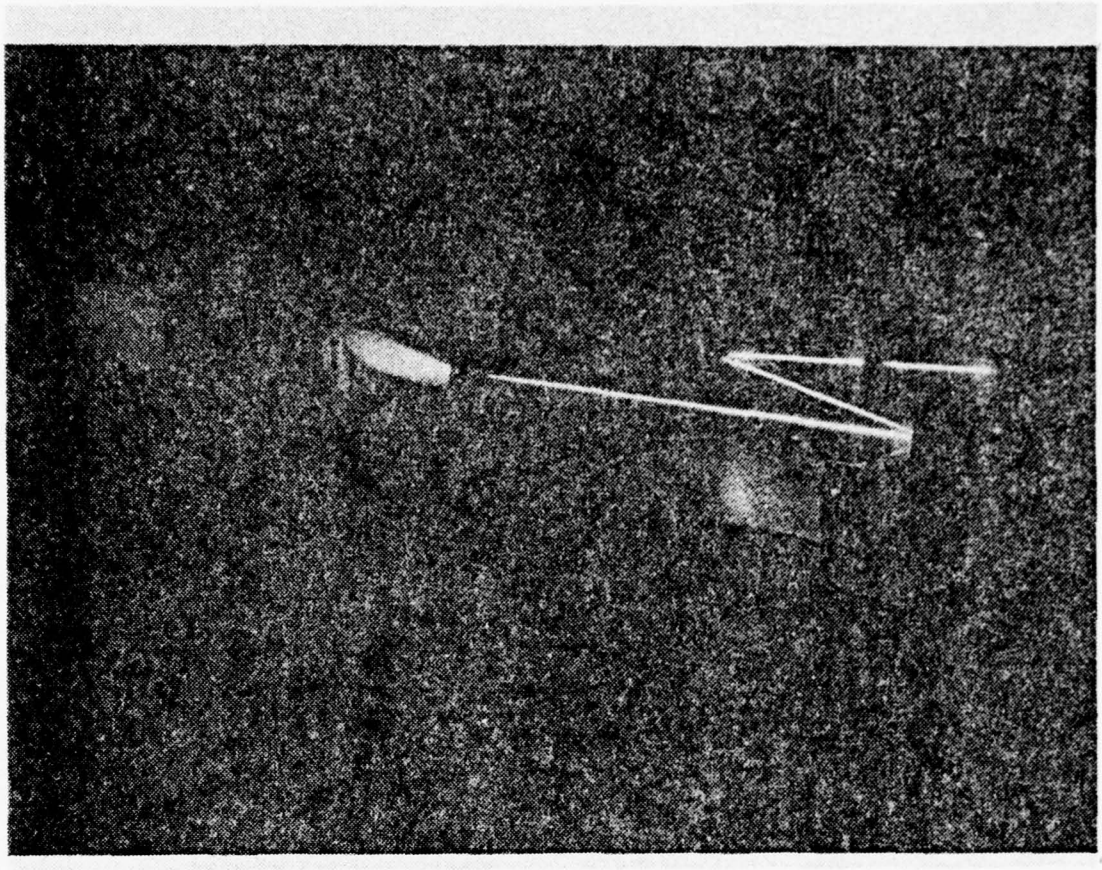

c) Holographic System with Laser Illuminating the Reference Beam in a Dark Room

Figure 4. Vibration Isolation Table with Laser, Optical Components, and Test Specimen in Place

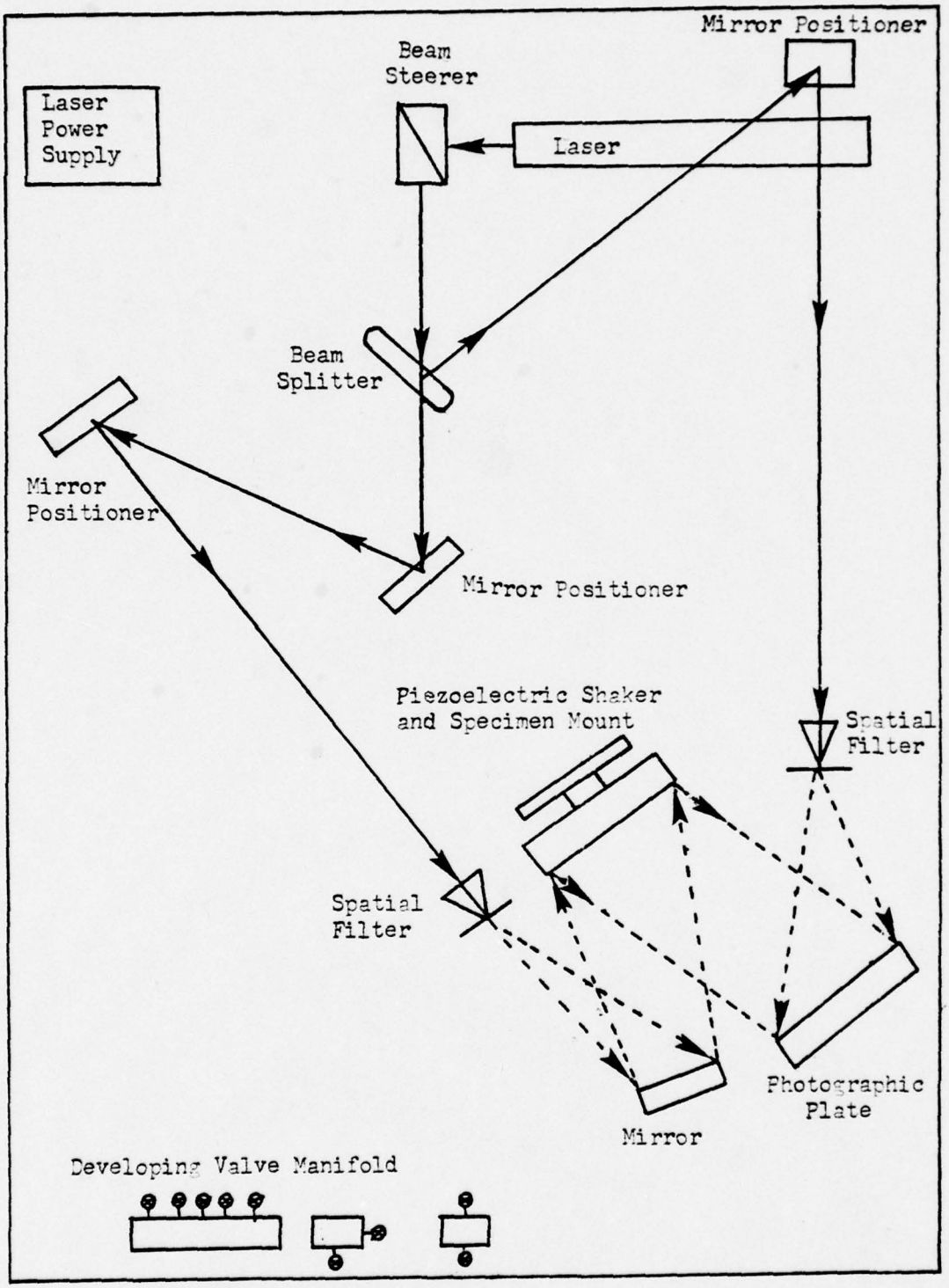

Figure 5. Schematic Diagram of Holographic System

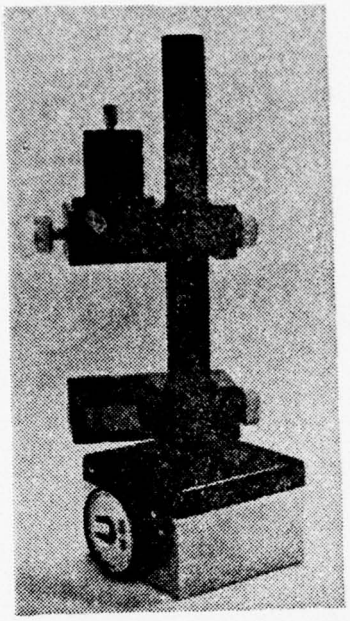

a) Beam Steerer

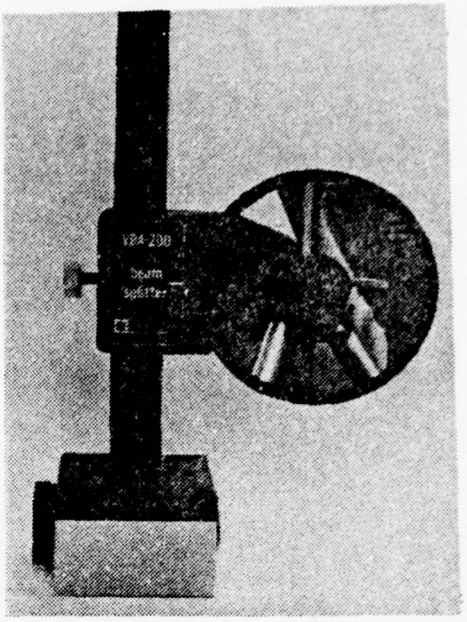

b) Variable Beam Splitter

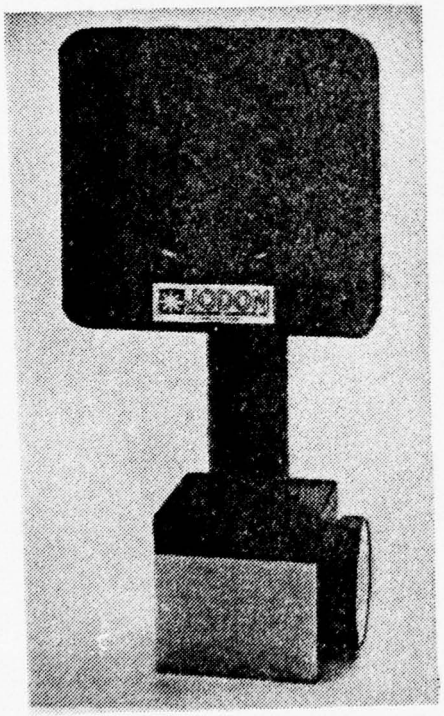

c) Mirror Positioner

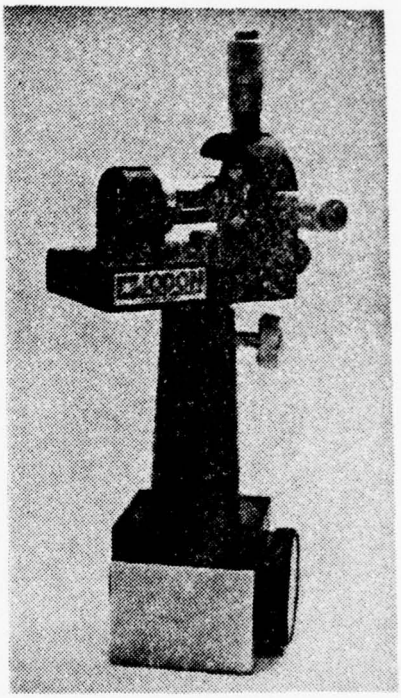

d) Spatial Filter

Figure 6. Holographic Optical Components

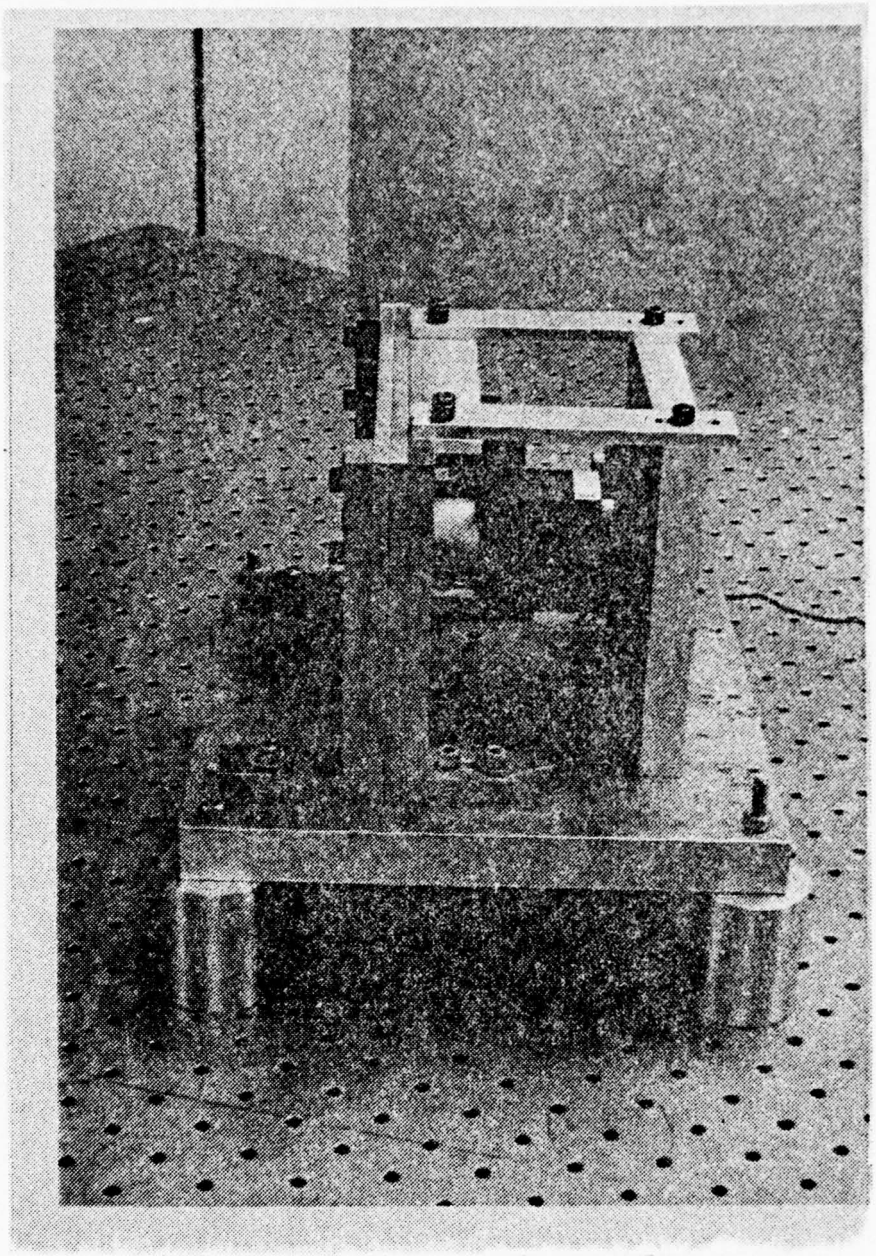

Figure 7. Piezoelectric Shaker and Test Speciment Mount

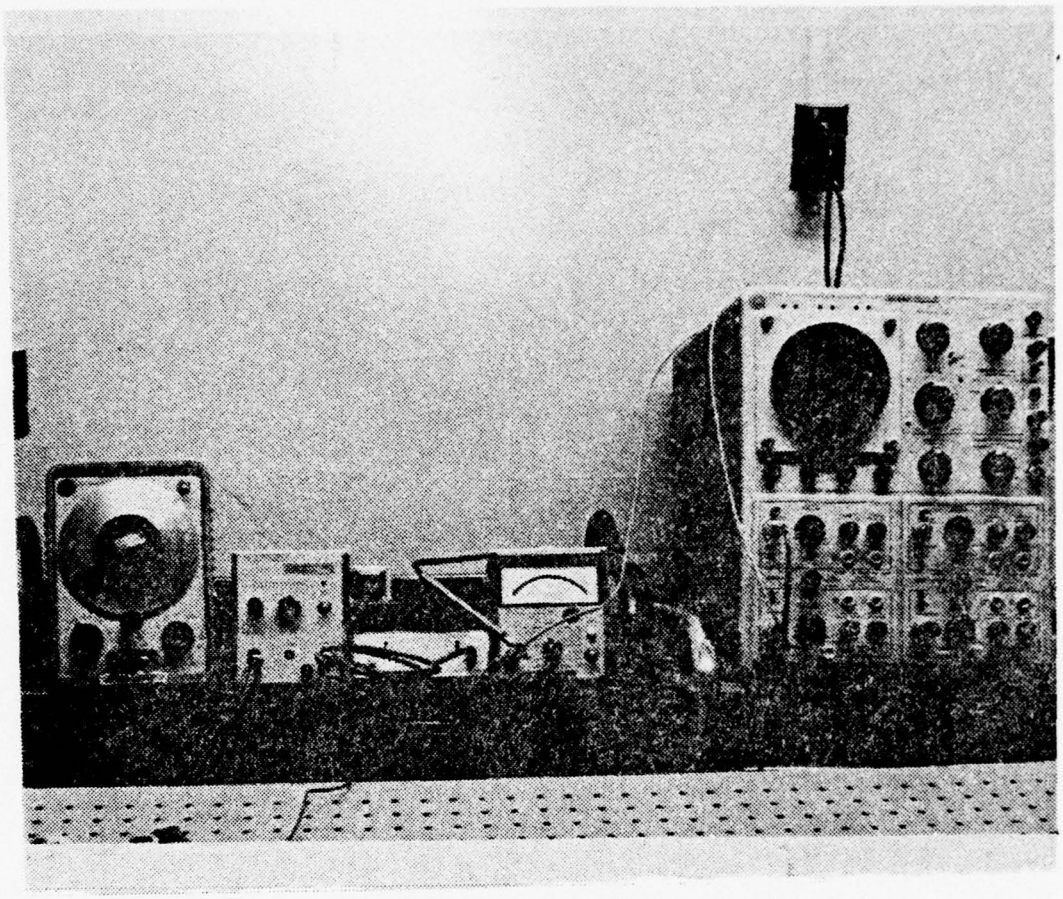

Figure 8. Piezoelectric Shaker Drive and Monitoring System

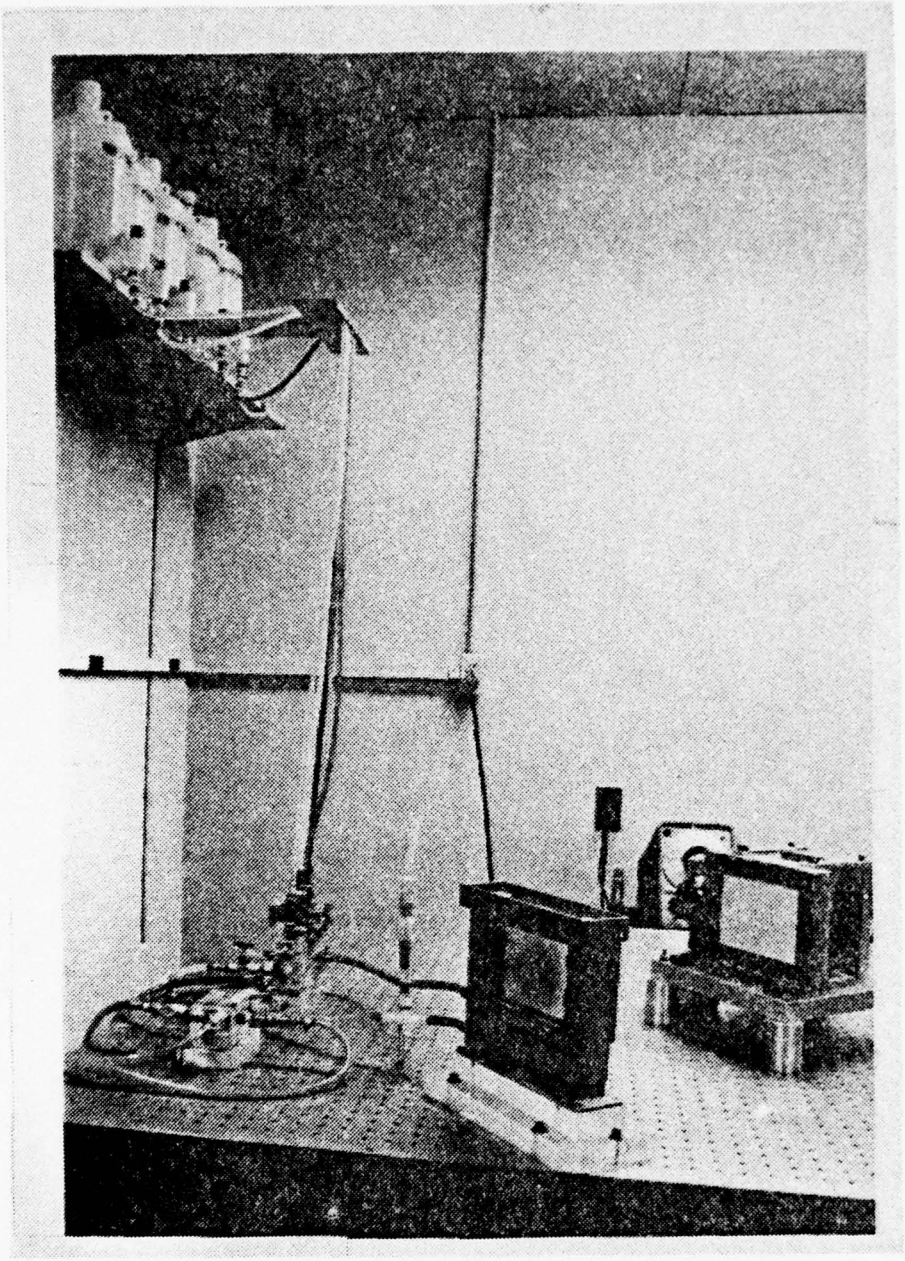

Figure 9. Photographic Plate Development System

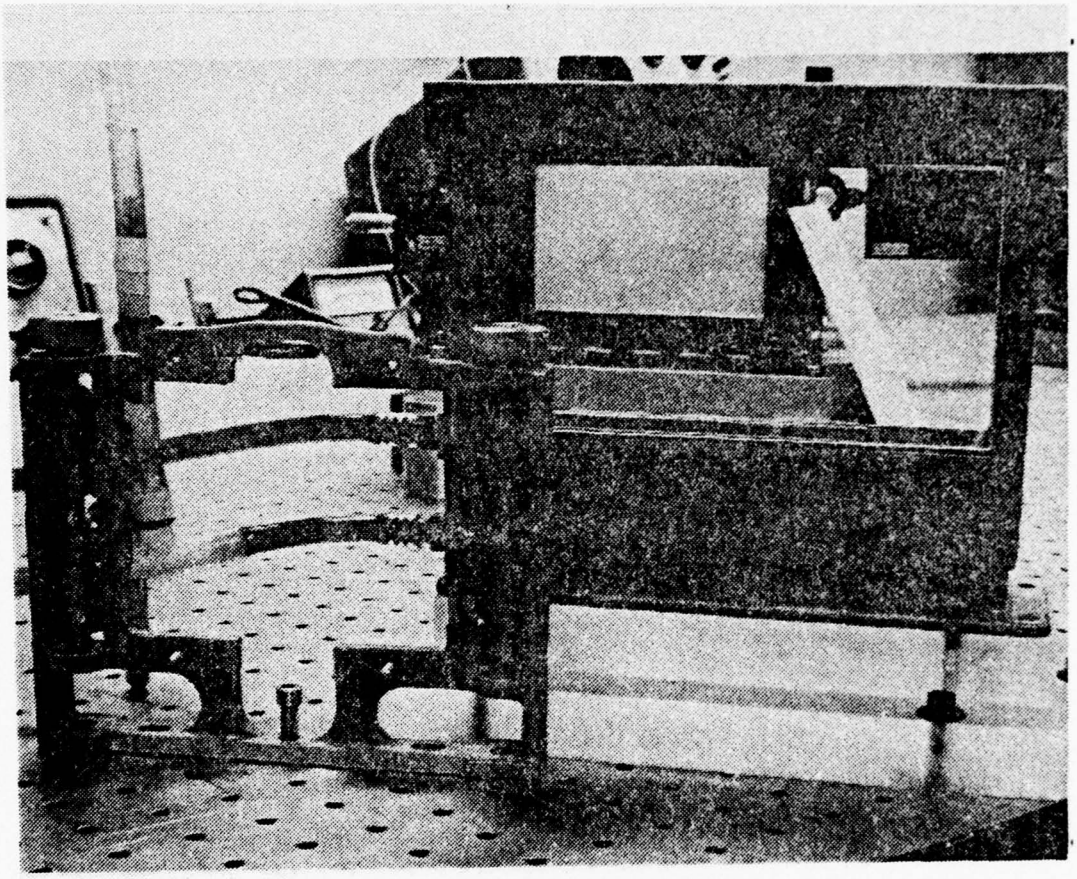

Figure 10. Photographic Plate Holder, Developing Tank, and Valve Manifolds

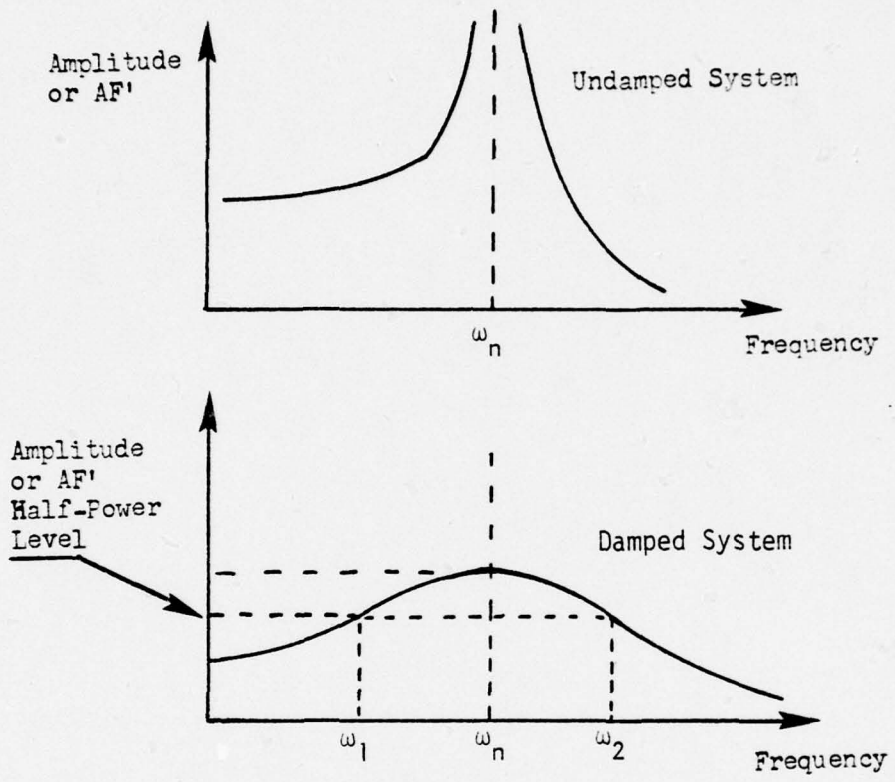

Figure 11. Influence of Damping on Response (Reproduced from Edwards [12])

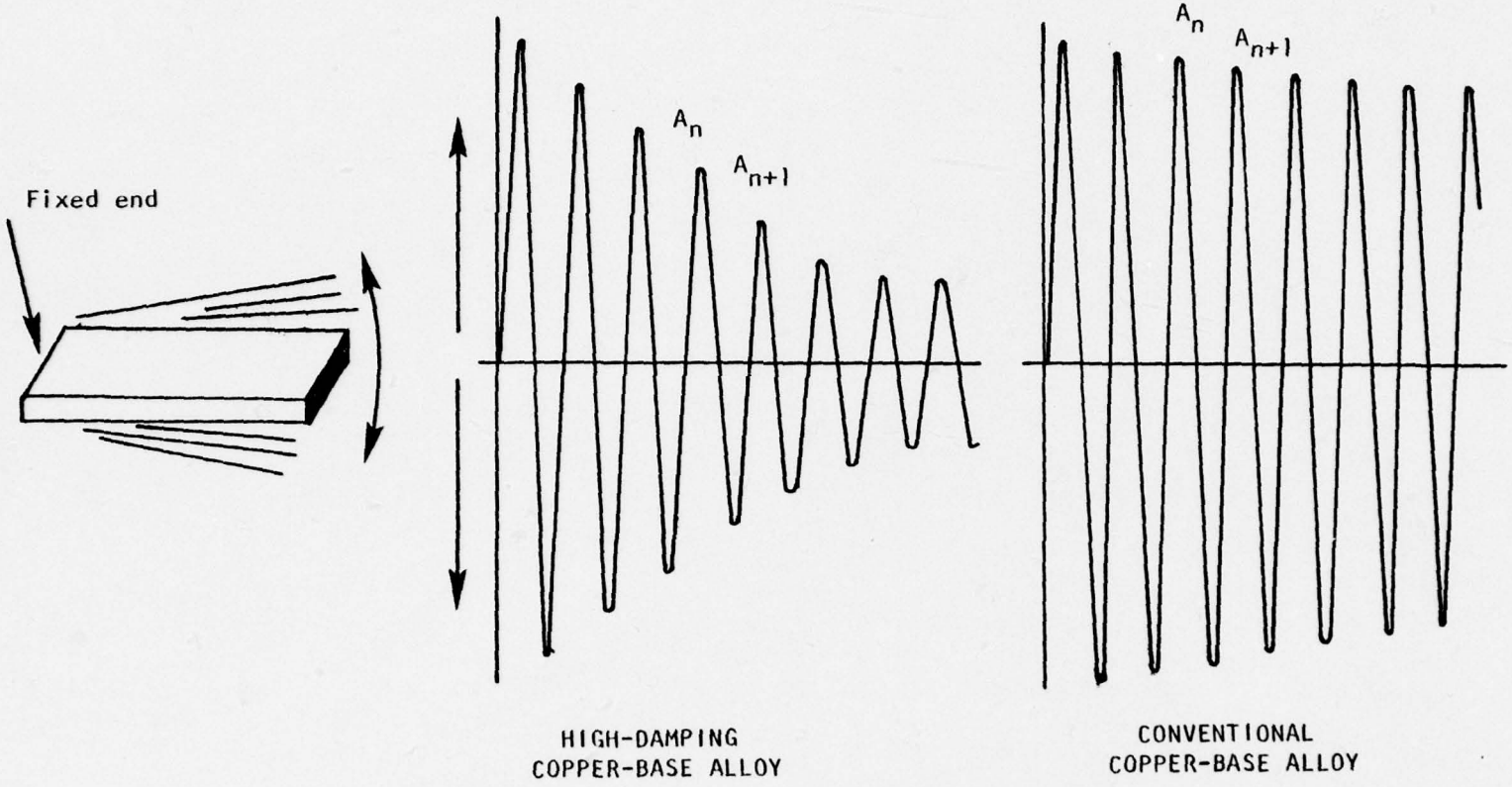

Figure 12. Experimental Method for Determining Specific Damping Capacity (Reproduced from Perkins [7])

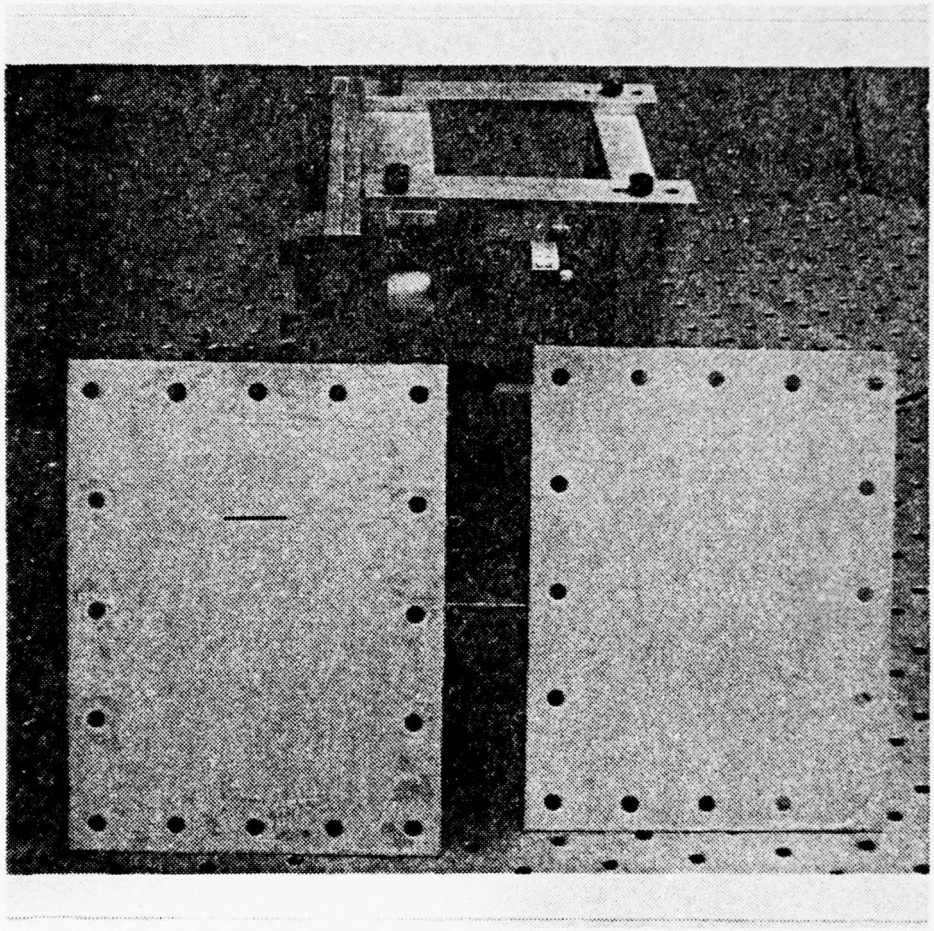

Figure 13. Aluminum 2024-T4 Test Specimens

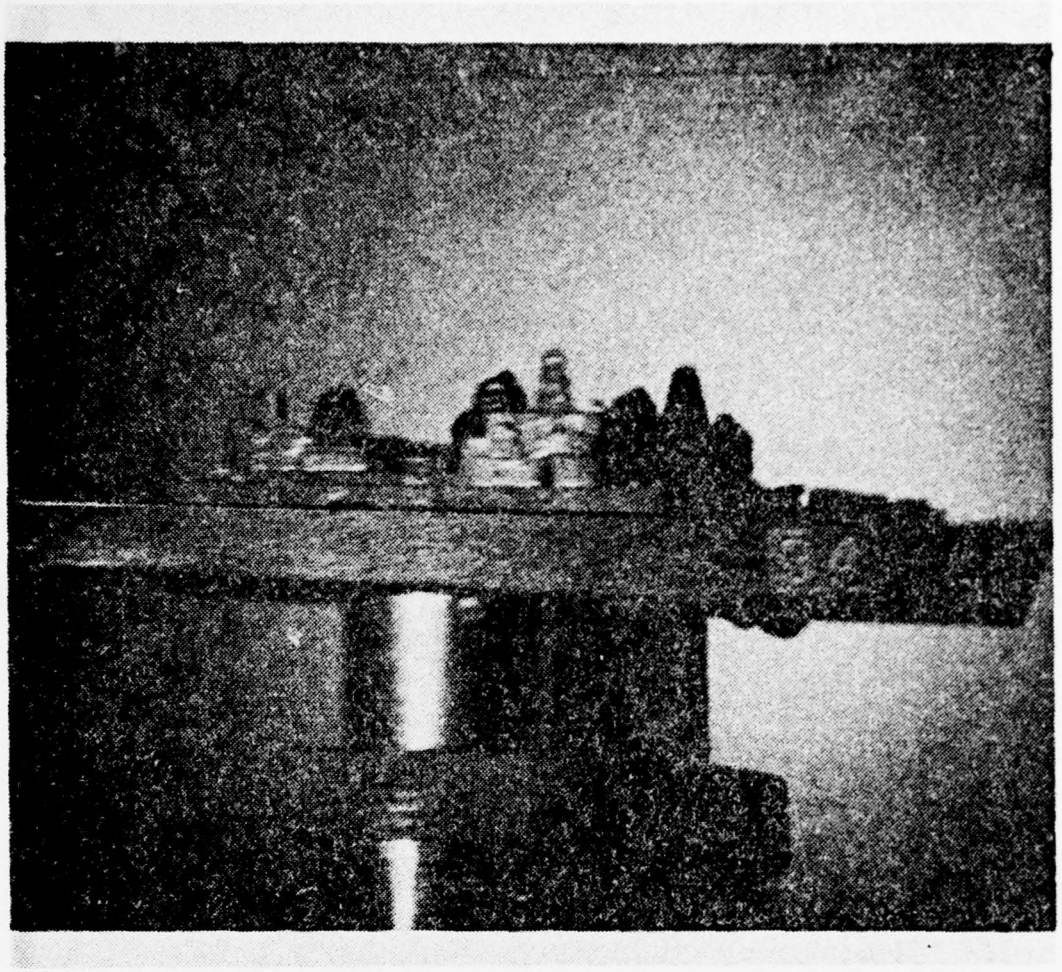

Figure 14. Hologram of Model Destroyer

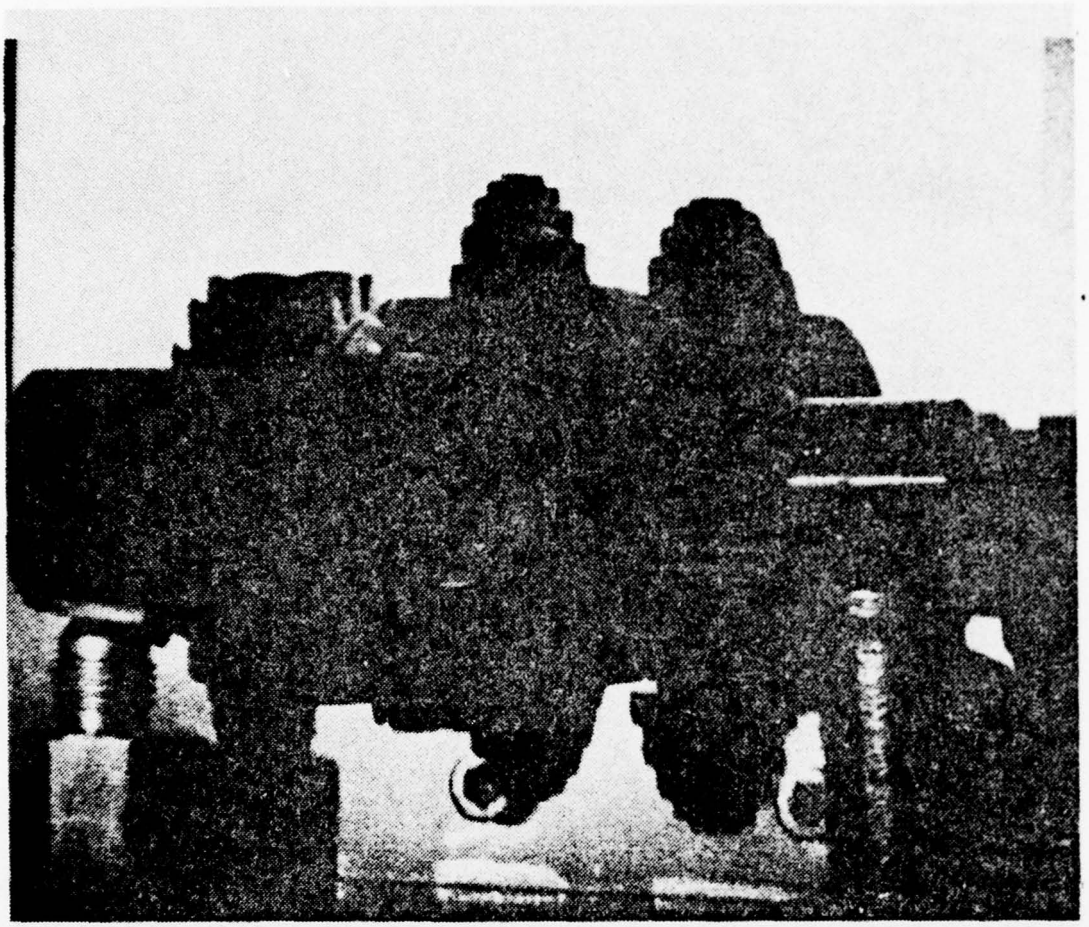

Figure 15. Hologram of Gear Assembly

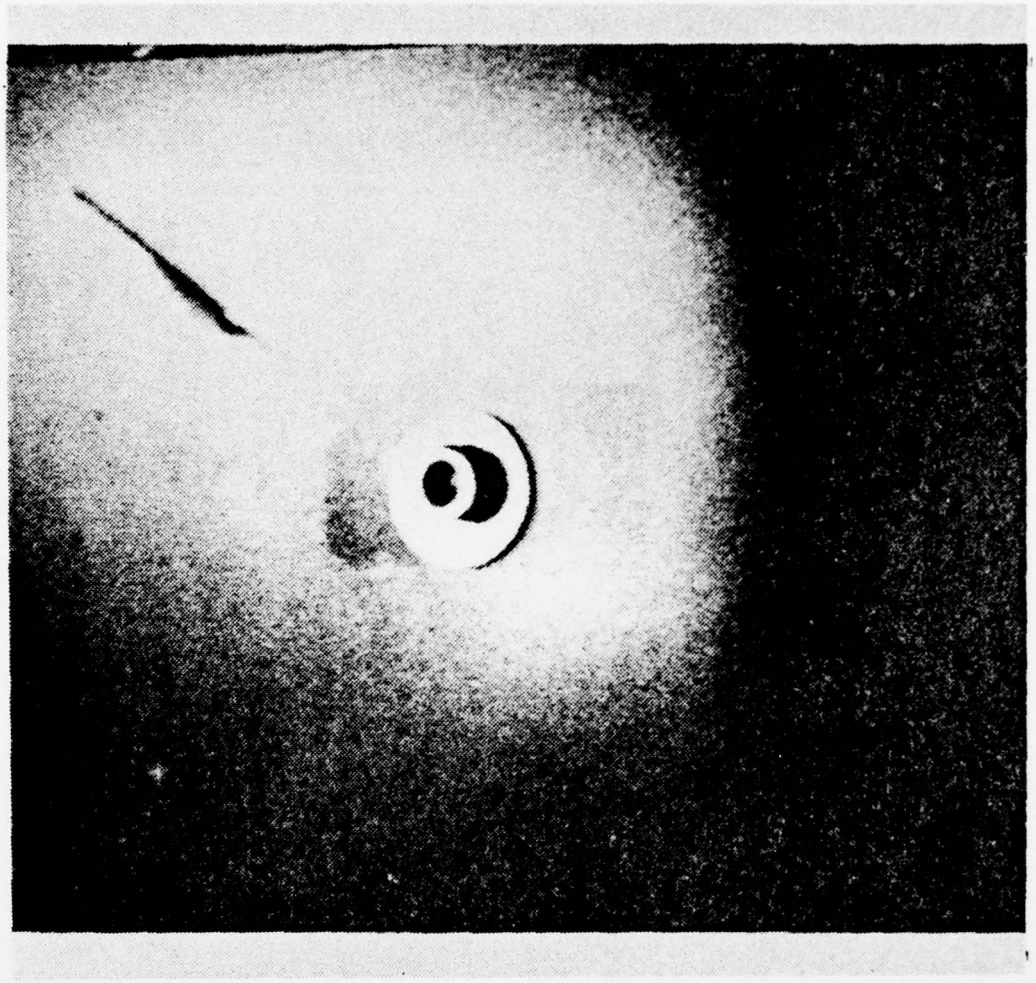

Figure 16. Hologram of Plate with Bolt and Flaw

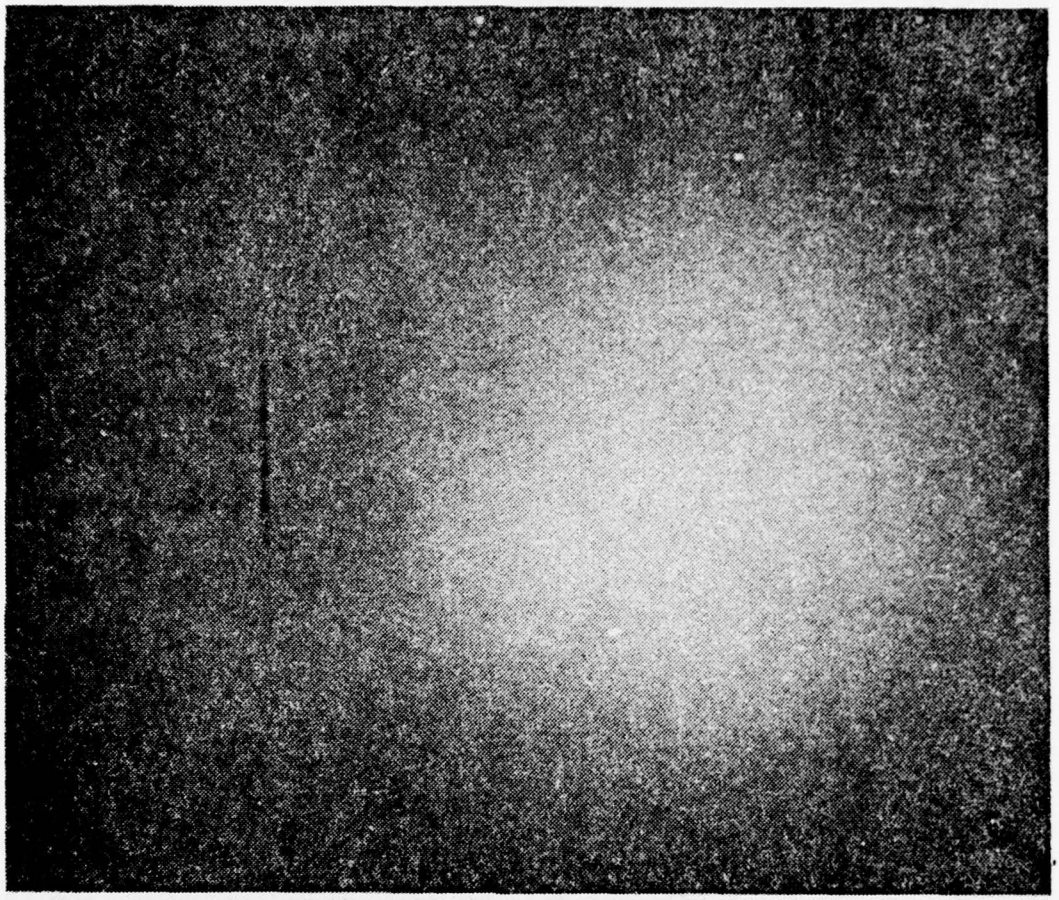

Figure 17. Hologram of Plate Prior to Vibration

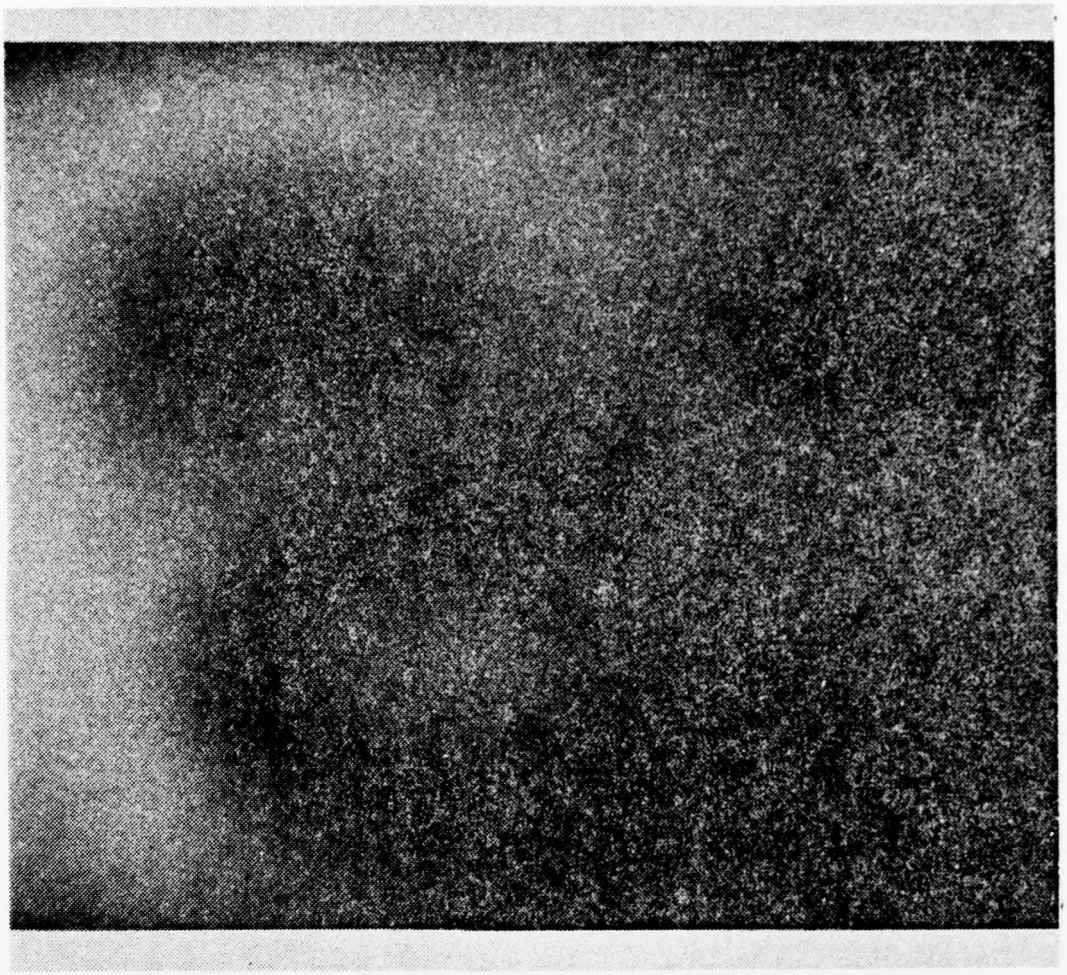

Figure 18. Double-Exposure Hologram of Plate at Theoretical Fundamental Frequency (m=1, n=1) of 327 HZ

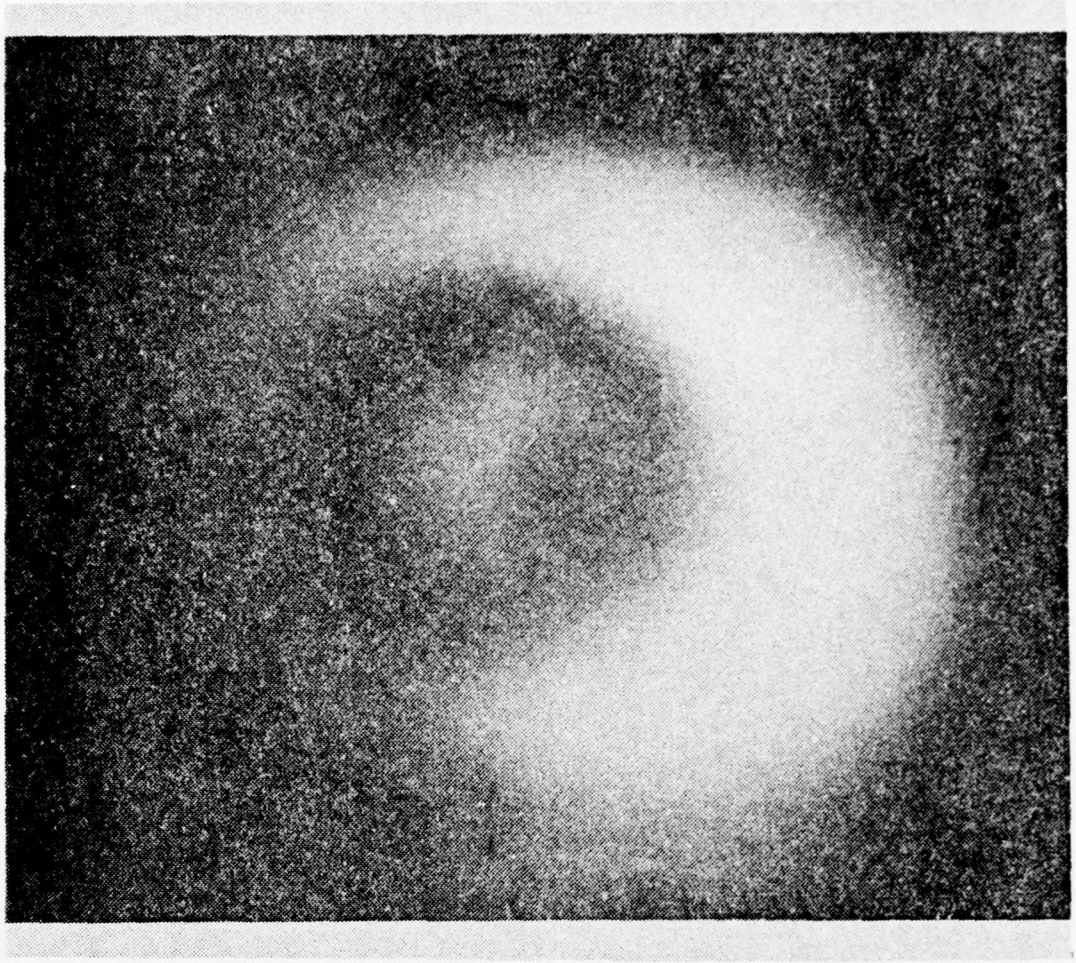

Figure 19. Double-Exposure Hologram of Plate at Fundamental Frequency (m=1, n-1) of 324 HZ

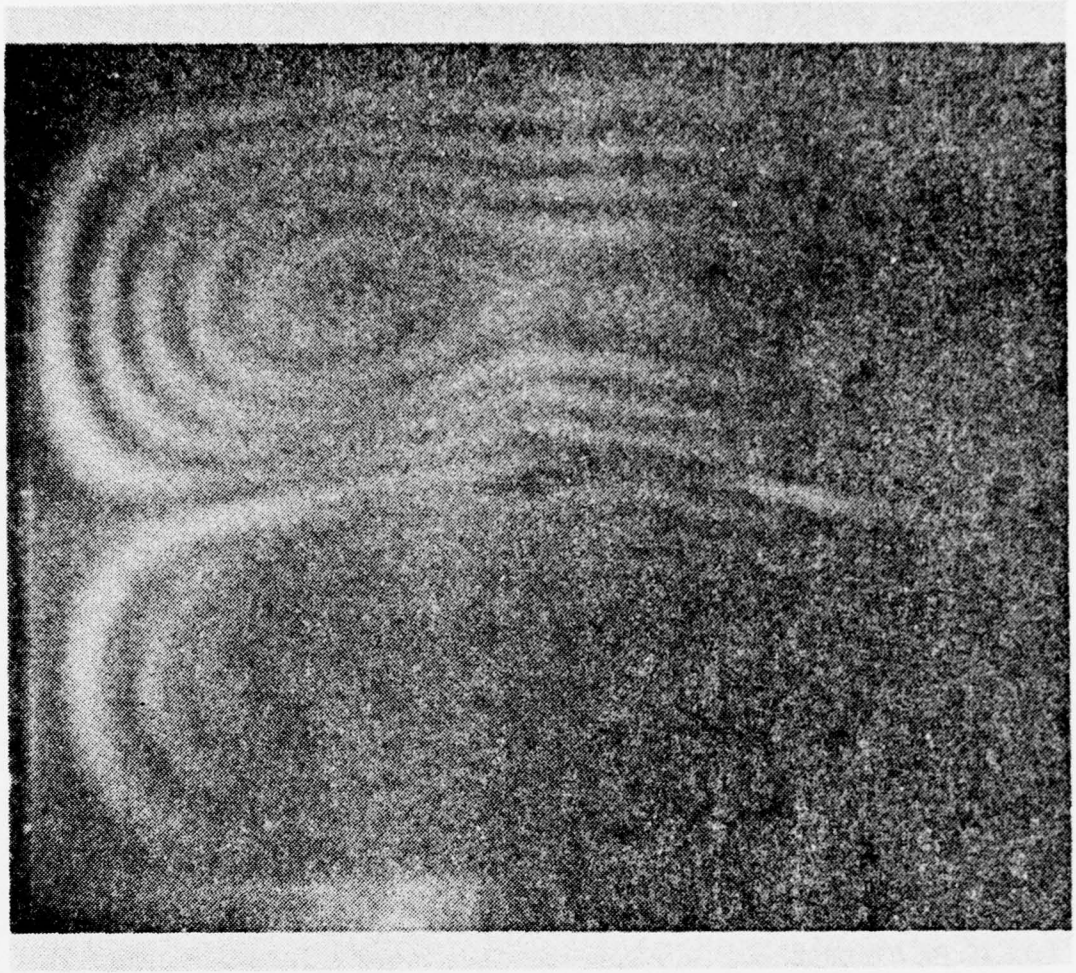

Figure 20. Double-Exposure Hologram of Plate at m=2, n=1 of 792 HZ

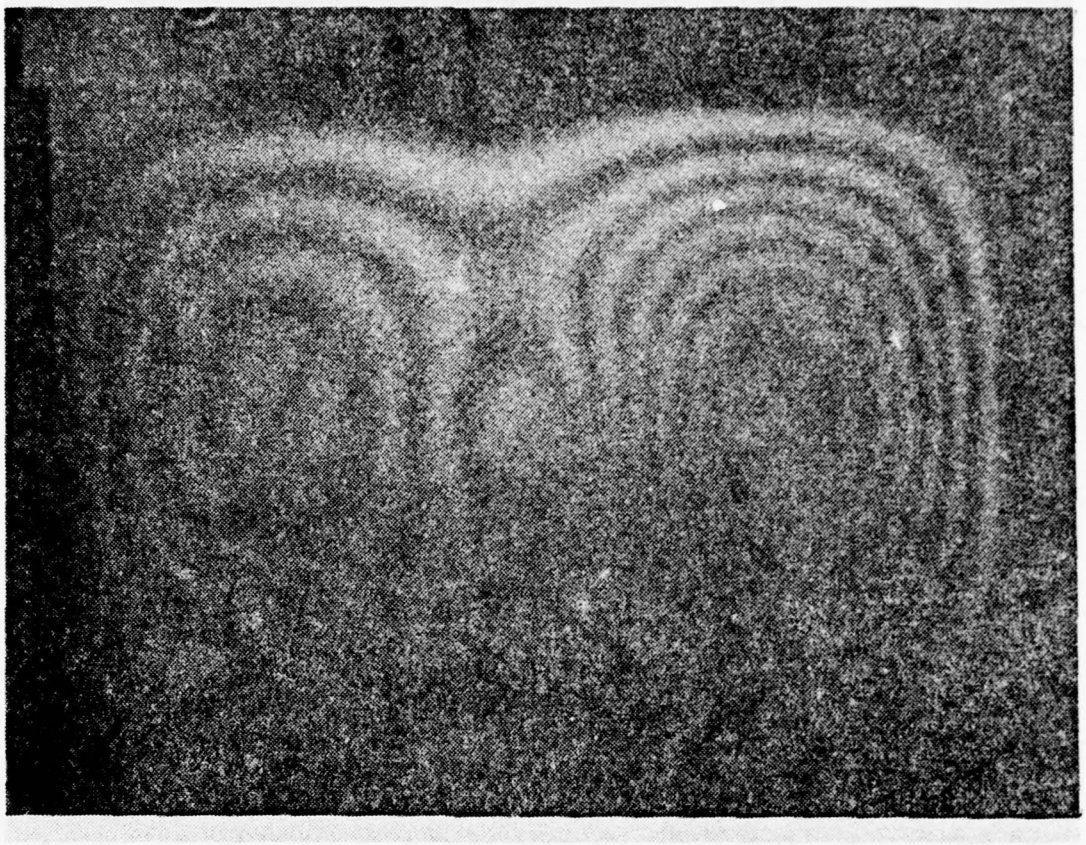

Figure 21. Double-Exposure Hologram of Plate at m=1, n=2 of 568 HZ

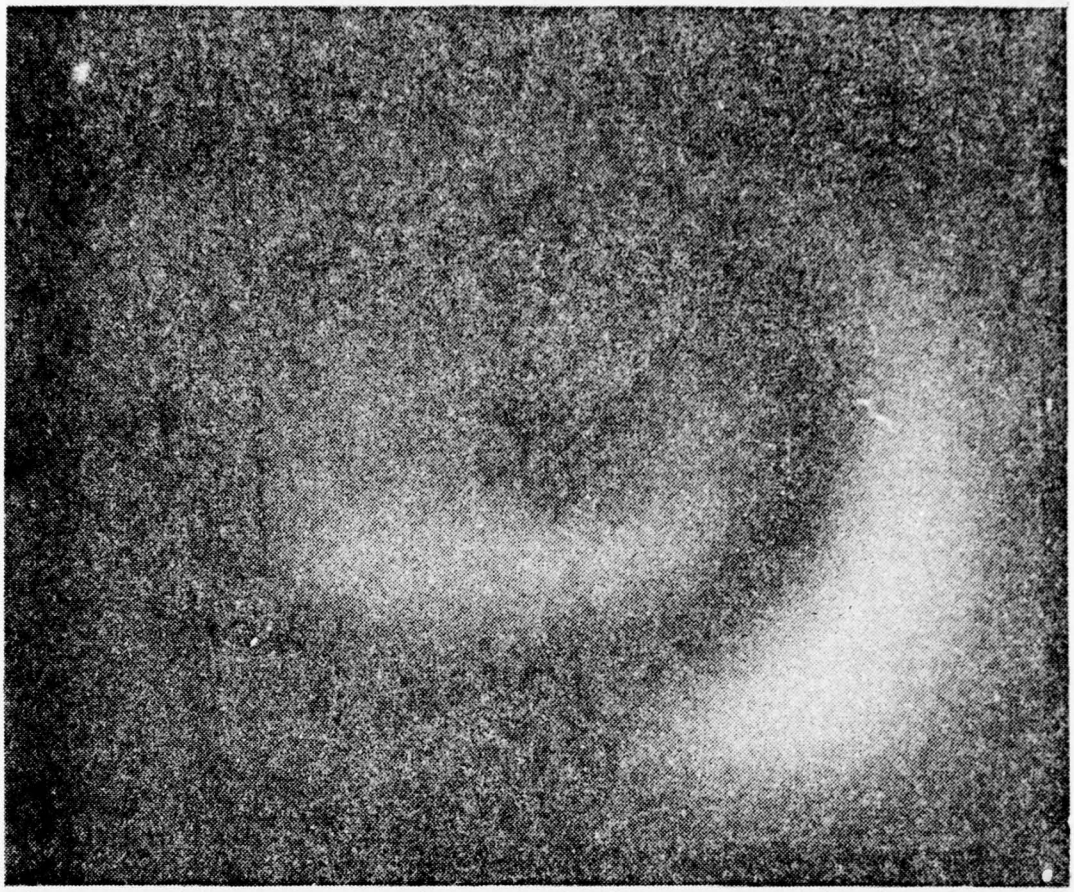

Figure 22. Double-Exposure Hologram of Flawed Plate at m=1, n=1 of 342 HZ

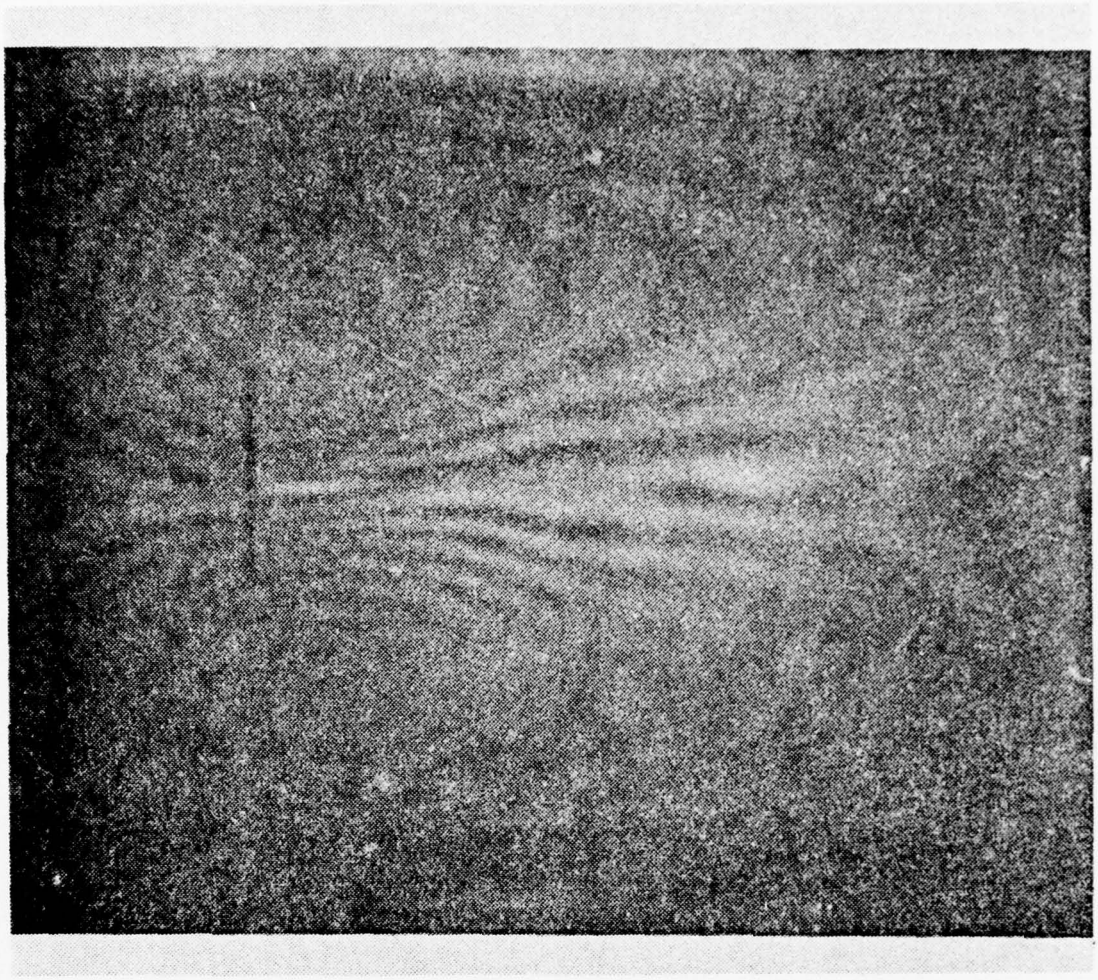

Figure 23. Double-Exposure Hologram of Flawed Plate at m=2, n=1 of 772 HZ

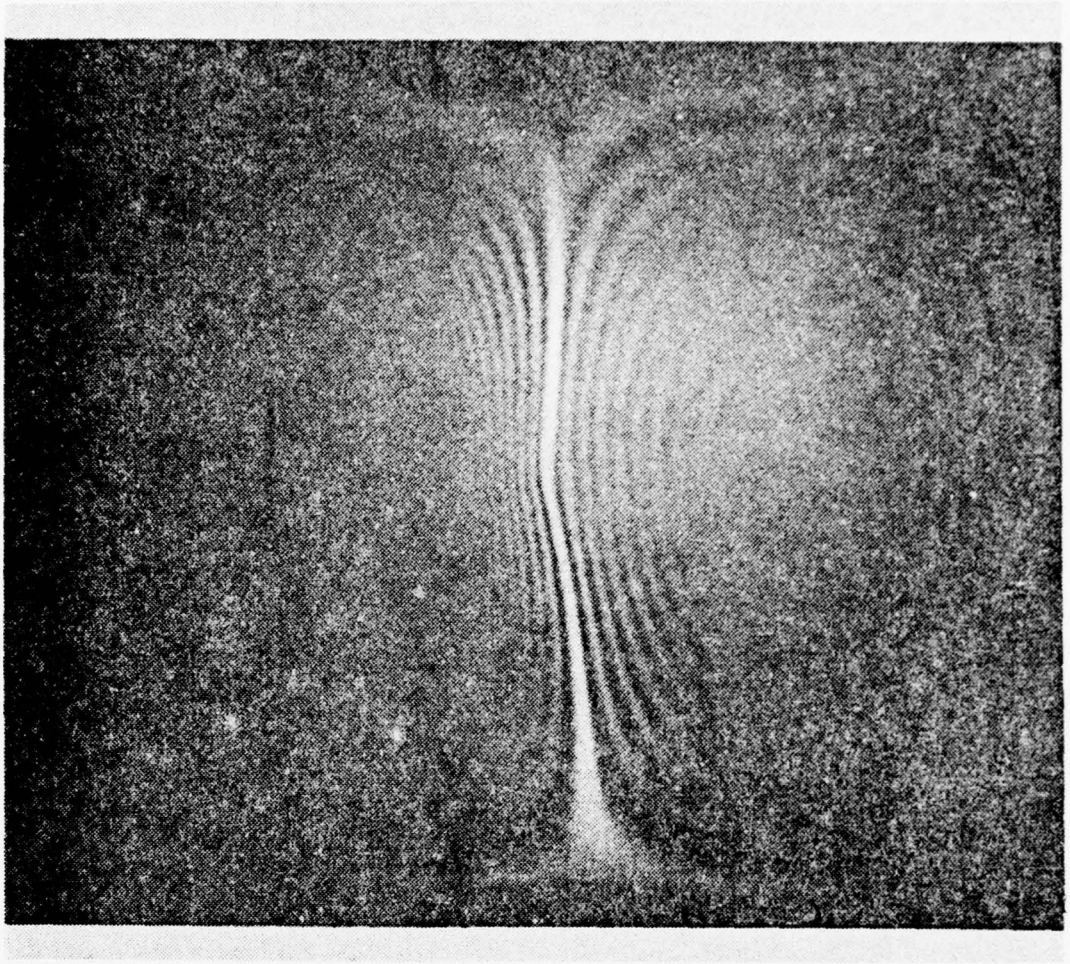

Figure 24. Double-Exposure Hologram of Flawed Plate at m=1, n=2 of 468 HZ

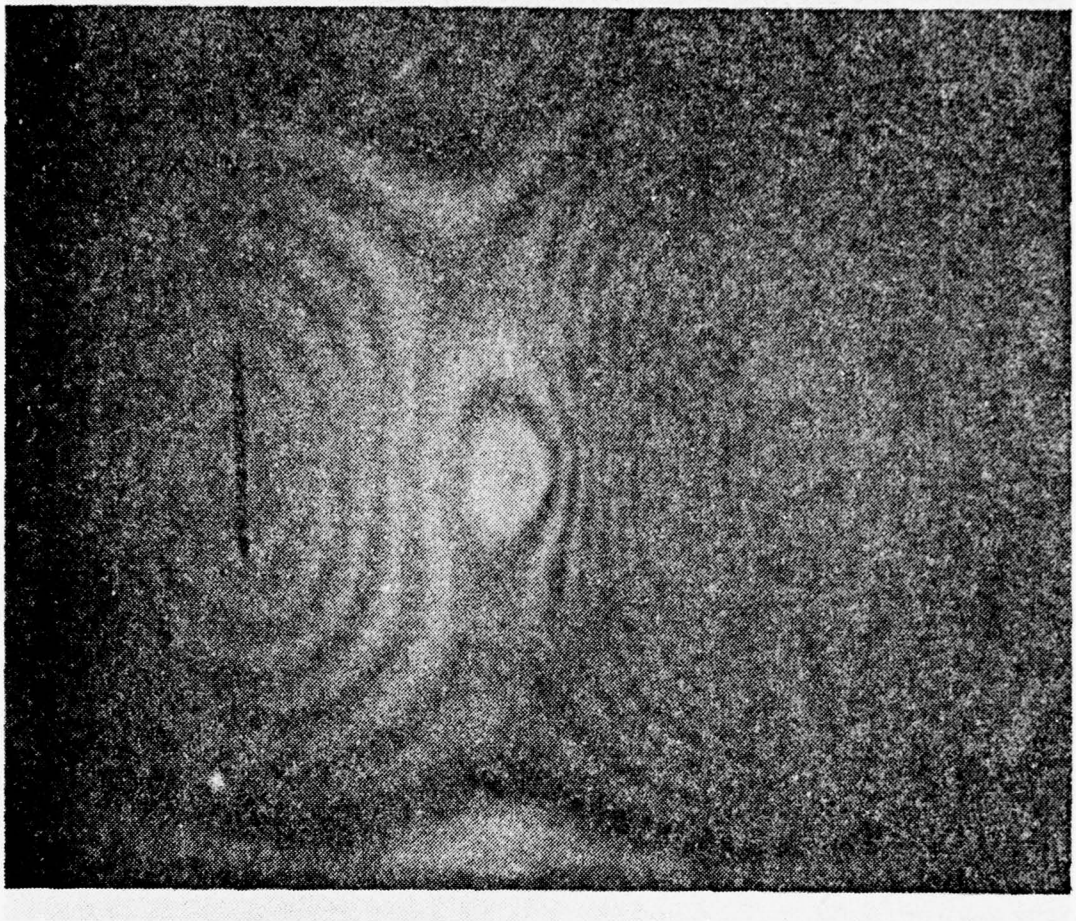

Figure 25. Double-Exposure Hologram of Flawed Plate at m=1, n=2 of 532 HZ

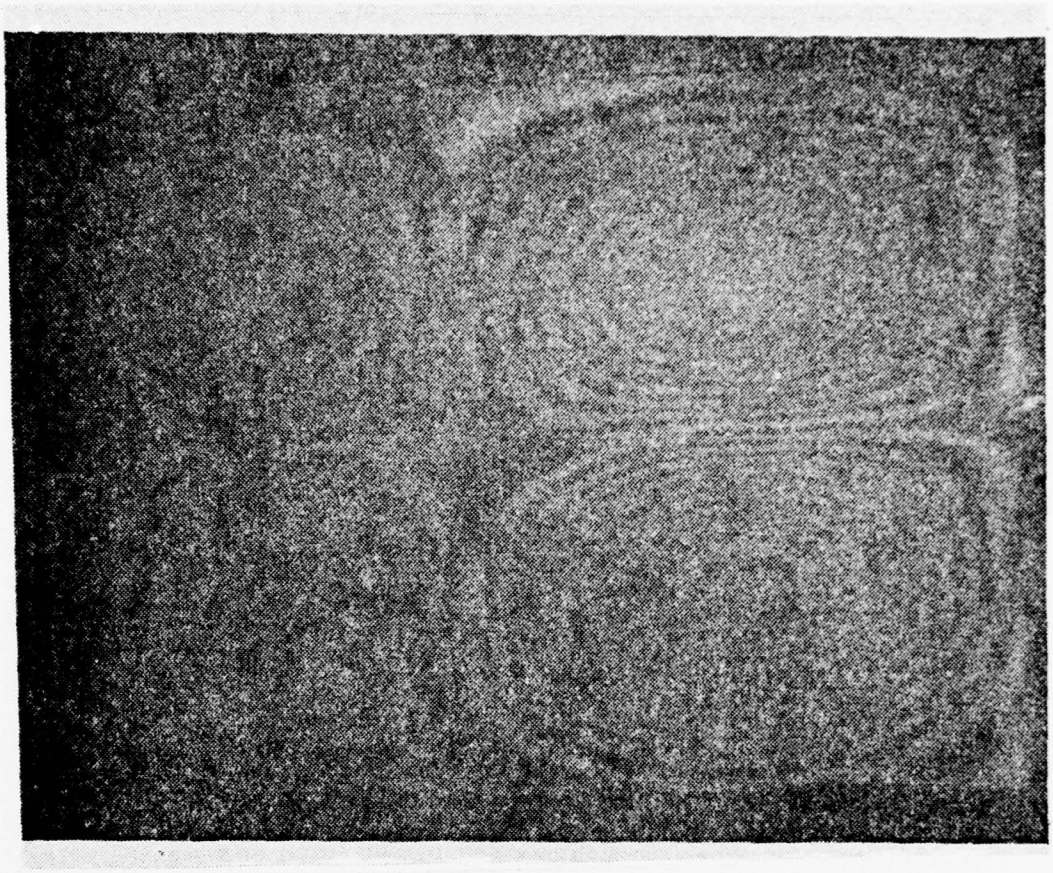

Figure 26. Double-Exposure Hologram of Flawed Plate at m=2, n=2 of 862 HZ

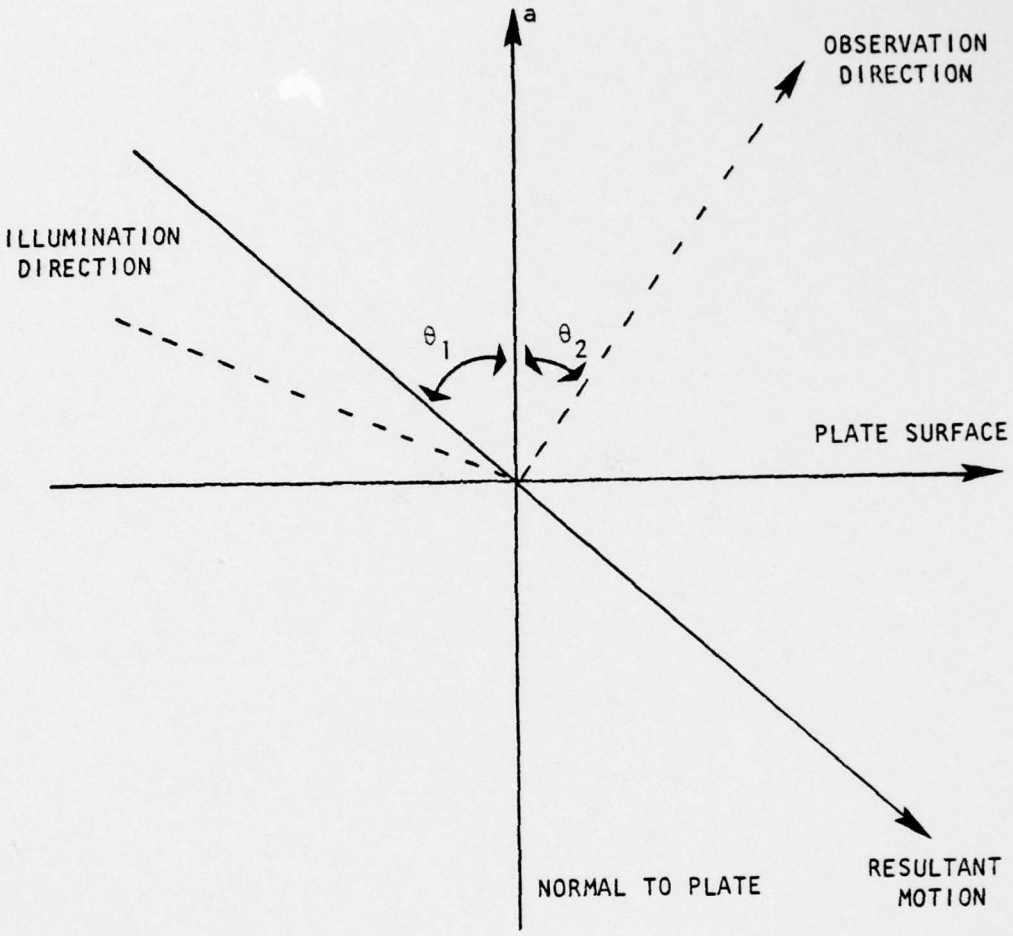

Figure 27. Orthogonal Components of Vibration at a Single Frequency

AD-A073 457 NAVAL POSTGRADUATE SCHOOL MONTEREY CA F/G 20/11
VIBRATION ANALYSIS AND NONDESTRUCTIVE TESTING USING DOUBLE-EXPO--ETC(U)
JUN 79 J M FAHEY

UNCLASSIFIED NL

2 OF 2
AD A073457

END
DATE FILMED
10-79
DDC

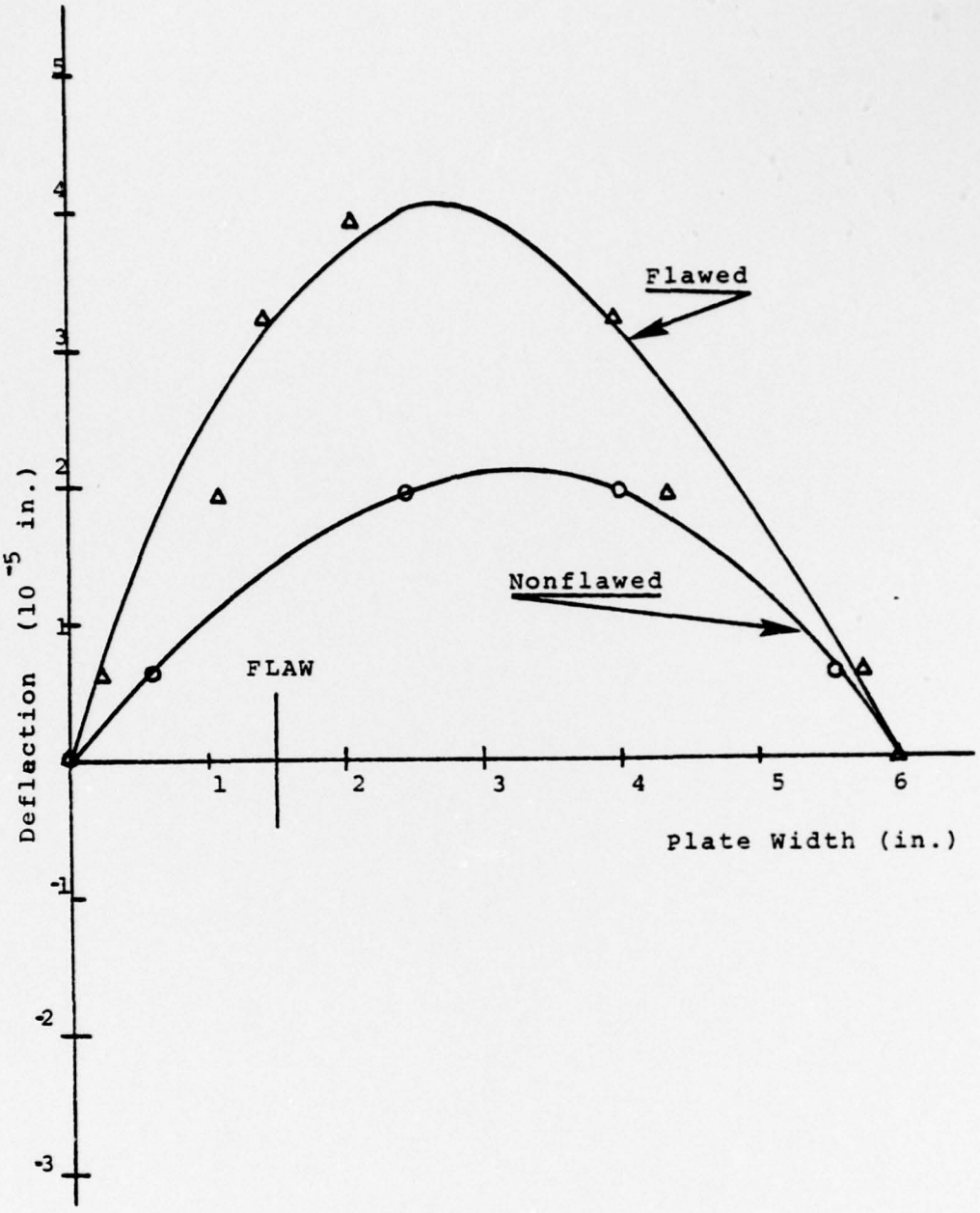

Figure 28. Fringe Deflection Curves for Flawed and Nonflawed Plates at m=1, n=1 Mode Shape

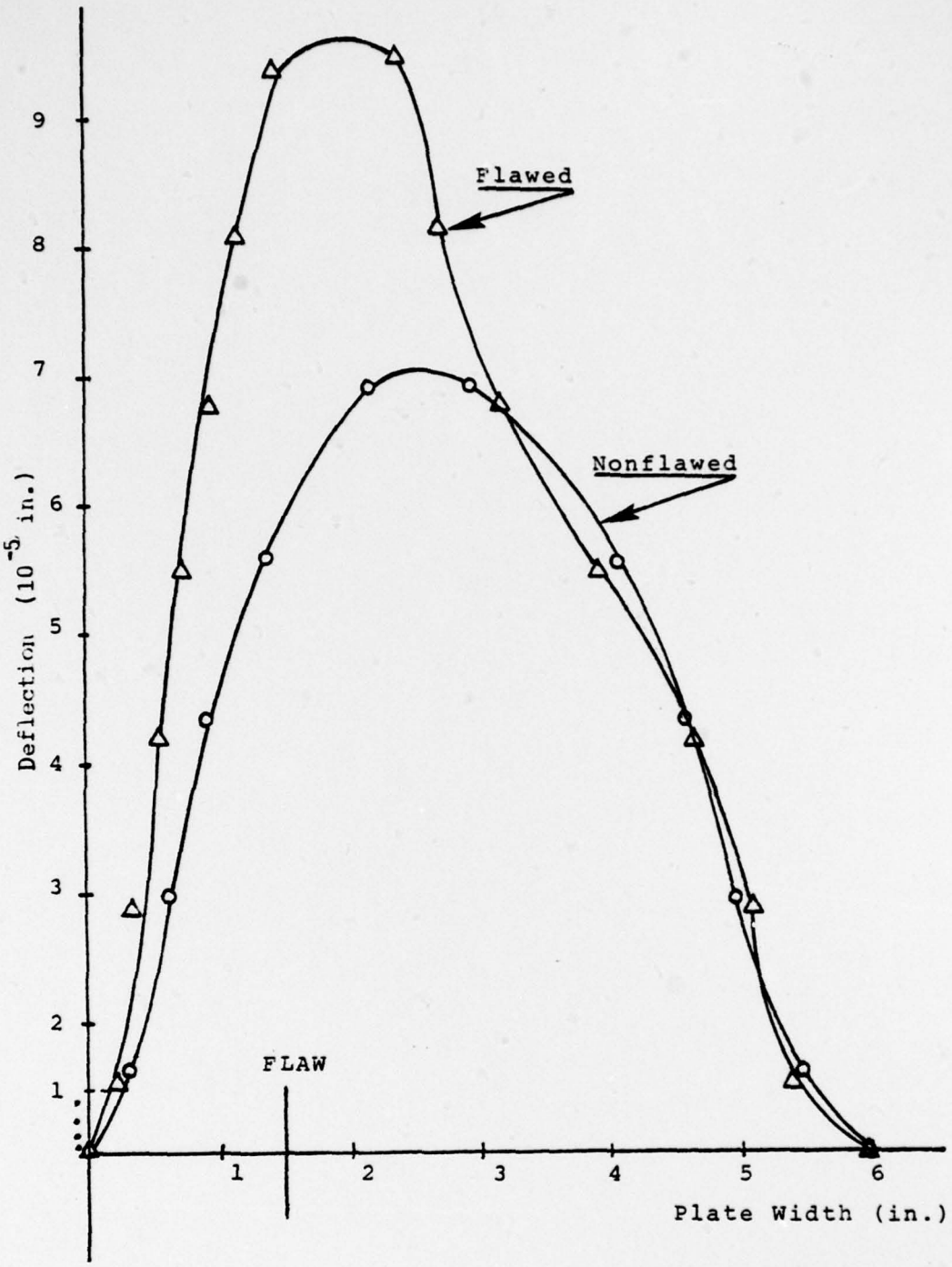

Figure 29. Fringe Deflection Curves for Flawed and Nonflawed Plates at m = 2, n = 1 Mode Shape

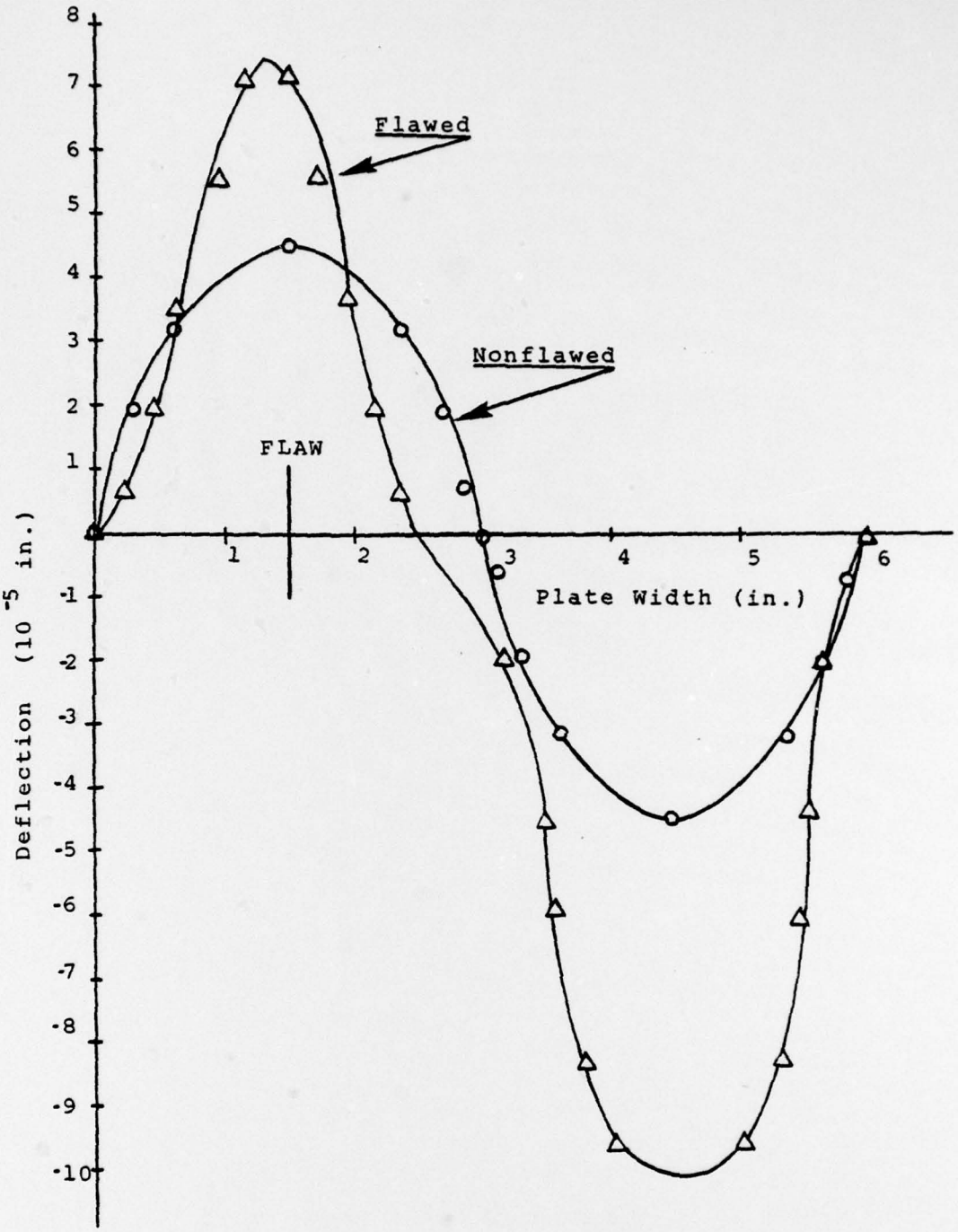

Figure 30. Fringe Deflection Curves for Flawed and Nonflawed Plates at m=1, n=2 Mode Shape

Table I. Specific Damping Capacities of Structural Materials

MATERIAL	SDC (%)
Magnesium (wrought)	49
Iron	16
Grey Cast Iron	6
Austenitic Stainless Steel	1
Aluminum Alloy 2024-T4	< 0.2

Table II. Summary of Results

MODE (a) m	n	Resonant Frequency (HZ) Without Flaw Theory	Without Flaw Experimental	Flaw
1	1	327.8	324.0	342.0
2	1	794.0	792.0	772.0
1	2	506.2	578.0	462.0(b) 532.0(c)
2	2	968.5		862.0

(a) See Leissa, [8], for definitions of m and n.

(b) Right side of flawed plate at resonant frequency

(c) Left side of flawed plate at resonance

APPENDIX A

MANIFOLD SYSTEM OPERATIONS

A. PROCEDURE TO BE FOLLOWED TO FLUSH AND OPERATE THE CHEMICAL SYSTEM

1. Utilize Distilled Water.

2. At the start of the procedure, the valve system as shown in Figure A-1 is lined up as follows:

Valve No.	Position
No. 1	Closed
No. 2	Closed
No. 3	Closed
No. 4	Closed
No. 5	Closed
No. 6	Closed
No. 7	Open
No. 8	Open
No. 9	Open

3. Crack Valve No. 1, and ensure a flow is present through Blowdown Valve No. 9.

4. Set the following lineup to fill the developing tank:

Valve No.	Position
1,7,8	Open
2,3,4,5,6,9	Closed

5. Fill the developing tank to above the inner overflow cell to ensure fluid flow. Once the desired water level has been achieved, secure Valve No. 1, light off the circulating pump to Position 10 (maximum capacity), and begin a 5-minute system flush.

6. Circulate with valves as follows:

Valve No.	Position
Nos. 1,2,3,4,5,6.9	Closed
Nos. 7,8	Open

Initially start circulating pump to No. 5 on the speed scale. Once flow has been ensured, set the dial to 10 on the indicator. At end of 5-minute flush, secure the pump, and drain the tank.

B. PROCEDURE TO DRAIN THE SYSTEM

Open Valve No. 9, and drain the developing tank contents into a discharge bottle below the isolation table.

C. PROCEDURE TO USE D-19 DEVELOPER

Follow the same procedures as for the flush (Part A) except the developing tank is filled with Kodak D-19 Developer by opening Valve No. 2. All other valves except Nos. 7 and 8 must be closed.

D. PROCEDURE TO USE KODAK STOP BATH

Follow the same procedures as for the flush (Part A) except the developing tank is filled with Kodak Stop Bath by opening Valve No. 3. All other valves except Nos. 7 and 8 are closed.

E. PROCEDURE TO USE KODAK FIXER

Follow the same procedures as for the flush (Part A) except the developing tank is filled with Kodak Fixer by opening Valve No. 4. All other valves except Nos. 7 and 8 are closed.

F. PROCEDURE TO USE METHANOL OR ETHYL ALCOHOL RINSES

Follow the same procedures as for the flush (Part A) except the developing tank is filled with Methanol or Ethyl Alcohol by opening Valve No. 5. All other valves except Nos. 7 and 8 are closed.

VALVE MANIFOLD SYSTEM

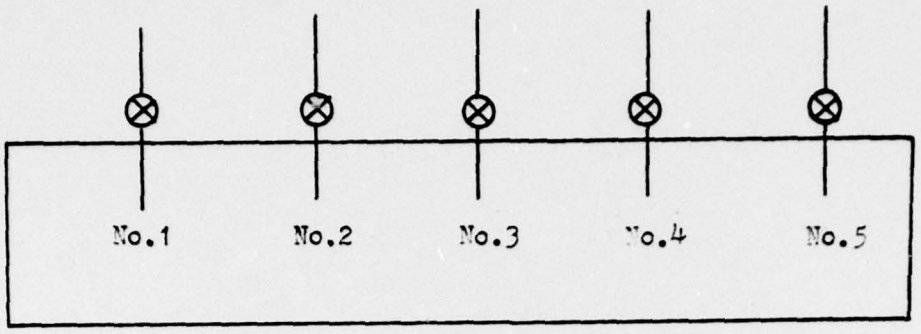

Valve No.	Solution
1	Distilled Water
2	Kodak D-19 Developer
3	Stop Bath
4	Fixer
5	Methanol or Ethyl Alcohol

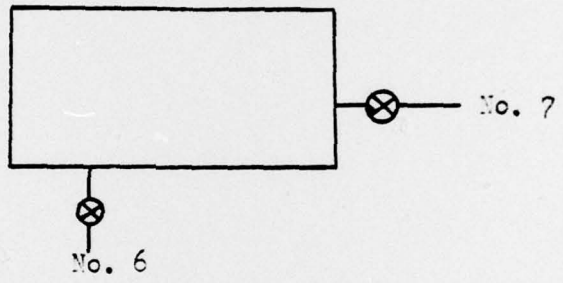

Valve No.	Function
6	System Blowdown
7	Circulation Pump Discharge

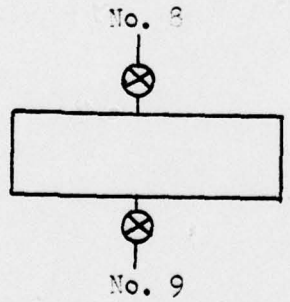

Valve No.	Function
8	Circulation Pump Suction
9	System Blowdown

Figure A-1. Valve Manifold System

APPENDIX B

PHOTOGRAPHIC SYSTEM

Once double-exposure holograms have been generated at various frequencies, the question of "What needs to be done next?" arises. In order to record the circumstances and analyze the data, a photographic image is necessary. This phase of the study posed minor problems because of the geometric constraints of the laboratory. The photographic system consists of a Polaroid 4x5 Land Film Holder #500 mounted in a Calumet Model C-1 Magnesium 8x10 View Camera with an ILEX Optical Company No. 5 Universal Synchro Lens with a focal length of 14.75 inches. The following discussion by Mack and Martin gives the necessary insight to lens theory [13].

To appreciate fully the importance of the term "focus" in the study, the concepts of focal length must be understood. Most lenses are made of glass, with one face ground to the shape of a portion of a spherical surface and the other ground to either a plane or spherical surface. The thick portion of a lens retards the central part of the beam more than the outer part causing the wave front to become spherical. The center of curvature of the wave front is then the point of convergence, or focus, of the beam, as shown in Figure B-1.

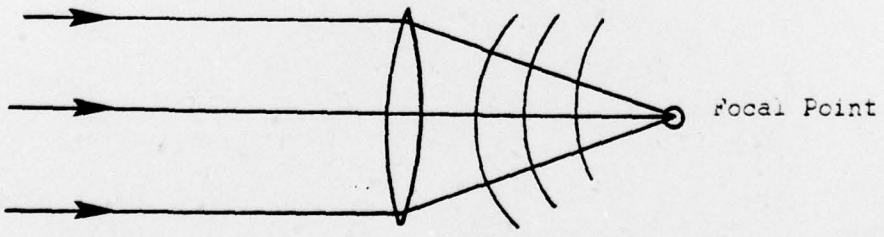

Figure B-1. Positive Lens

If the object is located at a finite distance from a convergent lens, the corresponding focal point would be located farther from the lens. This explains why a lens can alter the convergence by a specified amount. The original divergence of the light coming from an object near the lens tends to counterbalance the convergence resulting from the action of the lens. Also note that the greater the principal focal length of the lens, producing less converging power, the farther away will the image be formed for a given position of the object; see Figure B-2.

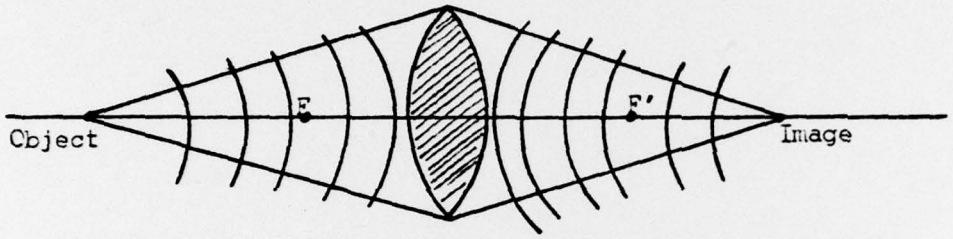

Figure B-2. Convergent Effect of a Lens on a Diverging Beam

The position and relative size of an image of an object at a given distance from a lens of known focal length can be determined by a geometrical construction. Figure B-3 describes the image formation for a positive (Convex) lens. Also note that it is customary in the science of photography to represent the object by an arrow with its tail on the principal axis.

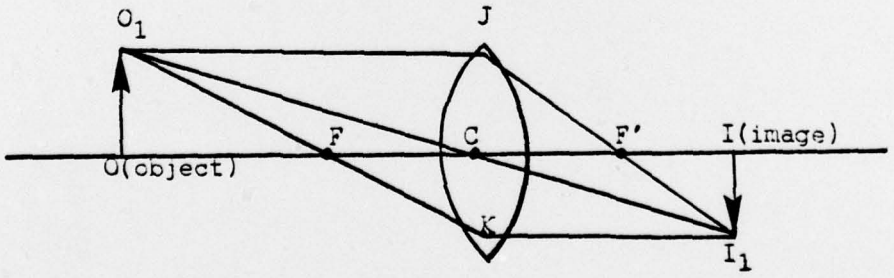

Figure B-3. Image Formation on a Positive Lens

The position of the image can be determined by tracing any two of the following three rays from the tip of the object arrow at point O_1:

(1) Ray O_1C through the optical center of the lens, which is undeviated.

(2) Ray O_1J parallel to the principal axis, which passes through the principal focus F'.

(3) Ray O_1K through the principal focus F which emerges parallel to the axis.

The intersection of these rays determines the point I_1, which is conjugate to O_1.

If the intersection that determines the image is not an intersection of the ray segments themselves but of their extensions backward from the instrument, the image is said to be virtual. A <u>virtual image</u> is then said to be one in which light does not pass but appears to pass. A virtual image can be caught on a screen but must be viewed by looking through the lens towards the object. A virtual image is associated generally with a negative lens as shown in Figure B-4.

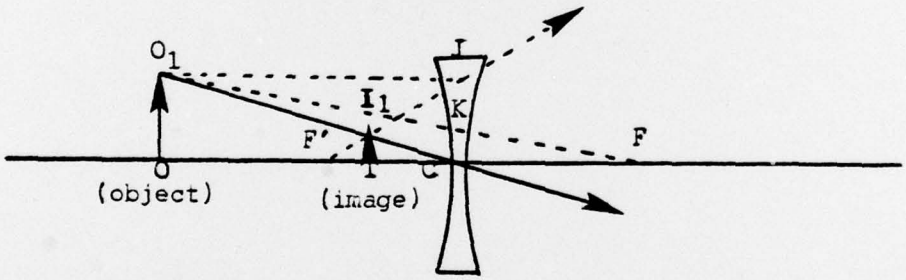

Figure B-4. Image Formation on Negative Lens

A real image is one represented by the positive lens figures where light actually converges and can be seen on a screen.

The basic theory followed for setting up the photographic equipment is the lens equation. Referring to the diagrams for the image formations on positive and negative lens systems, it is found that in the similar triangles COO_1 and CII, the corresponding sides are proportional.

$$\frac{I\ I_1}{O\ O_1} = \frac{CI}{CO} \tag{B-1}$$

Also in triangles F^1CJ and $F^1I\ I$, substituting OO_1 for its equal of CJ produces

$$\frac{I\ I_1}{O\ O_1} = \frac{IF^1}{CF^1} \tag{B-2}$$

Therefore,

$$\frac{CI}{CO} = \frac{IF^1}{CF^1} \tag{B-3}$$

or

$$\frac{v}{u} = \frac{v - f}{f} \tag{B-4}$$

which when simplified gives the lens equation

$$\frac{1}{u} + \frac{1}{v} = \frac{1}{f} \tag{B-5}$$

where u = the object distance OC

v = the image distance CI

f = the principal focal length FC or CF'

Utilization of this theory enabled the author to set up the photographic system so that the system could be focused with relative ease. The limiting factors are the focal length of the lens and the physical constraints of the laboratory.

The focal length f = 14.75 inches for the No. 5 Universal Synchro Lens and the object distance are limited by the table edge and the hologram developing tank. For best system alignment to ensure that the camera does not make contact with the table, u ≈ 30.0 inches.

Since

$$\frac{1}{f} = \frac{1}{u} + \frac{1}{v}$$

and

$$v = \frac{(u)(f)}{u-f}$$

where: f = 14.75 inches

u = 30.0 inches

therefore

$$v = \frac{(14.75)(30.0)}{(30.0) - (14.75)} \text{ inches}$$

$$v = 29 \text{ inches}$$

Utilizing the above dimensions, the author was able to focus clearly the holograms for photographic reproduction and data analysis.

LIST OF REFERENCES

1. Nehrich, R. B., Voran, G. I., and Dessel, N. F., Atomic Light Lasers, pp 88-94, Sterling Publishing Co., Inc., 1967.

2. Hoffman, P. P., Vibration Analysis and Nondestructive Testing Using Holographic Techniques, MSME Thesis, Naval Postgraduate School, Monterey, California, 1978.

3. Smith, H. M., Principles of Holography, pp. 178-186, pp. 220-228, Wiley, 1975.

4. Born, M., and Wolf, E., Principles of Optics, p. 319, Pergamon Press, Ltd., London, 1959.

5. Erf, R. K., Editor, Holographic Nondestructive Testing, Academic Press, 1974.

6. Huber, P. M., Holographic Nondestructive Testing of Pipes, MSME Thesis, Naval Postgraduate School, Monterey, California, 1978.

7. Perkins, J., and Schetsky, L. M., "The Quiet Alloys," Machine Design, pp. 202-203, 6 April 1978.

8. Leissa, A. W., Vibration of Plates, pp. 58-65, National Aeronautics and Space Administration, 1969.

9. Tonin, R., and Bies, D. B., "Analysis of 3-D Vibrations from Time Averaged Holograms," Applied Optics, 1 December 1978.

10. Tuschak, P. A., and Allaire, R. A., Experimental Mechanics, 15, 81, March 1975.

11. Sikora, J. P., Determination of Displacements from Holograms Using Simply Applied Methods that Are Comparable to Speckle Techniques, David Taylor Naval Ship Research and Development Center-78/108, December 1978.

12. Edwards, G. R., Perkins, J., and Hills, N., Materials Approach to Ship Silencing, Naval Postgraduate School, Monterey, California, 1974.

13. Mack, J. E., and Martin, M. J., The Photographic Process, pp. 52-65, McGraw-Hill, 1939.

INITIAL DISTRIBUTION LIST

		No. Copies
1.	Defense Documentation Center Cameron Station Alexandria, Virginia 22314	2
2.	Library, Code 0142 Naval Postgraduate School Monterey, California 93940	2
3.	Department Chairman, Code 69 Department of Mechanical Engineering Naval Postgraduate School Monterey, California 93940	1
4.	Professor A. E. Fuhs, Code 67Fu Department of Aeronautical Engineering Naval Postgraduate School Monterey, California 93940	2
5.	LCDR Paul M. Huber, USN Portsmouth Naval Shipyard Portsmouth, New Hampshire 03801	1
6.	Commander Boston Naval Shipyard ATTN: Code 130 Boston, Massachusetts 02129	1
7.	Commander Puget Sound Naval Shipyard ATTN: Code 130 Bremerton, Washington 98314	1
8.	Commander Charleston Naval Shipyard ATTN: Code 130 Naval Base Charleston, South Carolina 29408	1
9.	Commander Long Beach Naval Shipyard ATTN: Code 130 Long Beach, California 90801	1
10.	Commander Pearl Harbor Naval Shipyard ATTN: Code 130 Box 400 Pearl Harbor, Hawaii 96860	1

11. Commander 1
Philadelphia Naval Shipyard
ATTN: Code 130
Philadelphia, Pennsylvania 19112

12. Commander 1
Portsmouth Naval Shipyard
ATTN: Code 130
Portsmouth, New Hampshire 03801

13. Commander 1
Norfolk Naval Shipyard
ATTN: Code 130
Portsmouth, Virginia 23709

14. Commander 1
Mare Island Naval Shipyard
ATTN: Code 130
Vallejo, California 94592

15. LT. Phil Hoffman, USN 1
Pearl Harbor Naval Shipyard
ATTN: Code 331

Pearl Harbor, Hawaii 96860

16. CAPT. Alfred Skolnick 1
Naval Sea Systems Command
PMS 405
Crystal City
Washington, D. C. 22202

17. RADM. James W. Lisanby 1
Naval Ship Engineering Center
NAVSEA 6000
N.C. 2 Crystal City
Washington, D. C. 22202

18. LCDR. J. M. Fahey, USN 4
PXO USS THORN (DD-988)
c/o FIT (Spruance Class)
Ingalls Shipbuilding Co.
Pascagoula, Mississippi 39567

19. Professor A. P. Boresi, Code 69Bh 2
Department of Mechanical Engineering
Naval Postgraduate School
Monterey, California 93940